Available online at www.sciencedirect.com
ScienceDirect
Solid State Communications 145 (2008) 502–506
solid state communications
www.elsevier.com/locate/ssc

Analysis of relationship between magnetic property and crystal structure of $La_{1-x}Sr_xCrO_3$ ($x = 0.13, 0.15$)

Yuhta Matsunaga[a], Fumihiko Nakamura[a], Hiroki Takahashi[b], Takuya Hashimoto[a,*]

[a] *Department of Integrated Sciences in Physics and Biology, College of Humanities and Sciences, Nihon University, 3-25-40, Sakurajousui, Setagaya-ku, Tokyo 156-8550, Japan*
[b] *Department of Physics, College of Humanities and Sciences, Nihon University, 3-25-40, Sakurajousui, Setagaya-ku, Tokyo 156-8550, Japan*

Received 20 April 2007; received in revised form 3 December 2007; accepted 10 December 2007 by T. Ando
Available online 15 December 2007

Abstract

Dependence of dc magnetization, M, of $La_{1-x}Sr_xCrO_3$ ($x = 0.13, 0.15$) polycrystalline specimens on external magnetic field, H, was measured at various temperatures. At higher temperatures above 274 K and 265 K for the specimens with $x = 0.13$ and 0.15, respectively, almost linear relationships were observed, indicating paramagnetic property. At the lower temperatures, hystereses, indicating canted antiferromagnetic property, were observed in M–H curves. The temperatures where the magnetic phase transition was observed showed agreement with those where base line shift was observed in differential scanning calorimetry (DSC) measurement. In the M–H curves of $La_{1-x}Sr_xCrO_3$ ($x = 0.13, 0.15$), saturation magnetization, M_s, was not observed at external magnetic fields as high as 70 kOe. At 226 K and 189 K for the specimens with $x = 0.13$ and 0.15, respectively, structural phase transition from orthorhombic- to rhombohedral-distorted perovskite was observed in DSC curves. At the temperature, abrupt decreases of residual magnetization, M_r, and variation of temperature dependence of coercive force, H_c, were detected. We regard that the abrupt decrease of M_r and the variation of temperature dependence of H_c at the structural phase transition temperature can be ascribed to discontinuous variation of Cr–O–Cr angles.

PACS: 75.30.Kz; 75.20.Ck

Keywords: A. Perovskite chromites; C. Crystal structure and symmetry; D. Magnetic property; D. Phase transitions

1. Introduction

It has been reported that oxides with distorted perovskite structure including 3d transition metal, $La_{1-x}Ae_xMO_3$, (Ae = Ca, Sr; M: 3d transition metal), have high functions such as high electrical conductivity at high temperatures under various gas atmospheres, catalytic property for decomposition of pollution gas, colossal magnetic resistance (CMR) and so on [1–3]. Especially, CMR of $La_{1-x}Ae_xMnO_3$ (Ae = Ca, Sr) attracts much interest toward new switching device and/or large scale memory by magnetic field [3]. For the application, information on the effect of oxygen nonstoichiometry, chemical state of the elements and crystal structure on magnetic property are essential. However, large difficulty could be prospected for experimental analysis for the effect of crystal structure on magnetic property of $La_{1-x}Ae_xMnO_3$, because not only crystal structure but also oxygen nonstoichiometry i.e. chemical state of Mn should be affected by not only Sr content but also preparation conditions [4]. In order to clarify the relationship between crystal structure of $La_{1-x}Ae_xMO_3$ (Ae = Ca, Sr, M: 3d transition metal) and magnetic property, oxide with no oxygen nonstoichiometry under normally employed preparation conditions, such as in air or in O_2, is desirable. $La_{1-x}Ae_xCrO_3$, (Ae = Ca, Sr) is the suitable candidate since no oxygen ion deficiency has been reported at temperature for preparation under log $P(O_2)$ of 0 to −5 [5–7], i.e. chemical state of Cr and concentration of holes and spins are determined by Ae content only. Moreover, Tezuka and coworkers carried out neutron diffraction of $La_{0.85}Sr_{0.15}CrO_3$ and observed magnetic Bragg peaks indicating that magnetic moment configuration

* Corresponding author. Tel.: +81 3 3329 1151x5516; fax: +81 3 5317 9432.
E-mail address: takuya@chs.nihon-u.ac.jp (T. Hashimoto).

0038-1098/$ - see front matter © 2007 Elsevier Ltd. All rights reserved.
doi:10.1016/j.ssc.2007.12.007

of the specimen was G-type originating from superexchange interaction between electrical spin on neighbouring Cr ions [8], which is analogous to that of $La_{1-x}Ae_xMnO_3$.

In the preceding paper [9], we have reported analysis of phase transition of $La_{1-x}Sr_xCrO_3$ by using differential scanning calorimetry (DSC), dilatometry, temperature-controlled X-ray diffraction and magnetic measurement using SQUID. Combining obtained data, structural and magnetic phase diagram of $La_{1-x}Sr_xCrO_3$, which includes paramagnetic orthorhombic, canted antiferromagnetic orthorhombic, canted antiferromagnetic rhombohedral and paramagnetic rhombohedral phase, has been proposed. In particular, two kinds of canted antiferromagnetic phase have been observed in the specimen with x larger than 0.12; one is orthorhombic-distorted, the other rhombohedral-distorted perovskite, showing agreement with the results of neutron diffraction of $La_{0.85}Sr_{0.15}CrO_3$, by which the electron spin configurations of both phases were proposed [8]. However, residual magnetization (M_r), and coercive force (H_c), which might be affected by crystal structure, has not been investigated because dependence of magnetization at constant external magnetic field on temperature was mainly measured by using SQUID and few measurements were carried out on variation of magnetization on external magnetic field in the previous studies.

In this paper, dependence of magnetization of $La_{1-x}Sr_xCrO_3$ ($x = 0.13$, 0.15) on external magnetic field were reported. The measurements were carried out at various temperatures and effect of structural phase transition on M_r and H_c has been investigated combining with DSC measurements and discussion on local structure around Cr^{3+}.

2. Experimental

The polycrystalline specimens $La_{1-x}Sr_xCrO_3$ ($x = 0.13$, 0.15) were prepared by Pechini method [10]. The starting materials were powdery La_2O_3 (99.9% Furuuchi Co., Ltd.), $SrCO_3$ (99.9% Furuuchi Co., Ltd.) and $Cr(NO_3)_3{\cdot}9H_2O$ (99.9%, Wako Chemical Co., Ltd). Prior to the preparation, La_2O_3 was heated in air at 1200 °C for 12 h to decompose small amount of impurities such as $La(OH)_3$ and $La_2(CO_3)_3$. $SrCO_3$ was dried in air at 120 °C for 6 h. These materials in a stoichiometric ratio were completely dissolved in dilute nitric acid. Then, excess citric acid was added to the solution to obtain the chelate of each metal. Posterior to addition of ethylene glycol, the solution was heated at about 300 °C. The solution changed to a polyester resin, which was burned to a powder. The obtained powder was calcined at 700 °C for 7 h in air and pressed into pellets of 20 mm diameter and 2–3 mm thick, which were successively sintered at 1400 °C for 24 h in air. After cooling, the obtained pellets were reground into powder in alumina mortar and pressed into pellets with 5 mm diameter again, which were sintered again at 1400 °C for 24 h in air. For powder X-ray diffraction measurement (Cu Kα; 50 KV, 250 mA, Rigaku RINT-2500) and difference scanning calorimetry (DSC; DSC8230, Rigaku Co., Ltd.), some of the obtained pellets were reground again into a powder in alumina mortar. DSC was carried out by using about 40 mg of powder specimen crimped in Al pan as a sample at a heating rate of 10 °C/min in Ar atmosphere. The measurement temperature range was −150–450 °C. Al_2O_3 powder also crimped in Al pan was used as a reference. X-ray diffraction measurement at room temperature indicated that the obtained specimens were single phase of rhombohedral-distorted perovskite. In the obtained DSC curves of $La_{1-x}Sr_xCrO_3$ ($x = 0.13$, 0.15), endothermic peak and baseline shift were observed at the temperatures, which showed correspondence with the phase diagram proposed in the previous study [9].

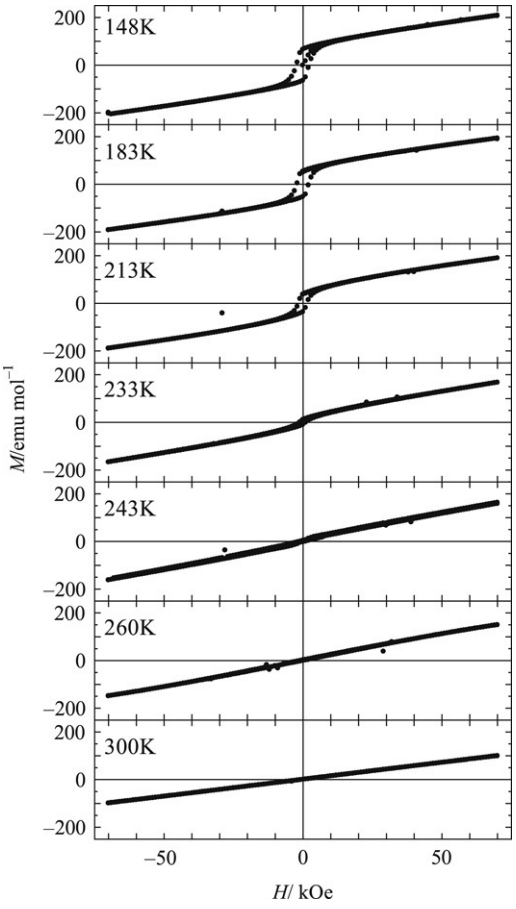

Fig. 1. Dependence of dc magnetization, M, on external magnetic field, H, of $La_{0.87}Sr_{0.13}CrO_3$ at various temperatures.

DC magnetization, M, of the sintered $La_{1-x}Sr_xCrO_3$ ($x = 0.13$, 0.15) were measured with a SQUID magnetometer (Quantum Design MPMS model). The temperature of the sample was controlled to measurement temperature under zero magnetic field and then susceptibility was measured by application of external magnetic field, H, between −70 and 70 kOe. The measurement temperature was 130–300 K.

3. Results

Fig. 1 shows representative M–H curves of $La_{0.87}Sr_{0.13}CrO_3$. Hysteresis originating from canted antiferromagnetic property was observed in M–H curve at 148 K. The DC magnetization, M, monotonically increased with increase of external field. Saturation of M was not observed up to 70 kOe, indicating canted antiferromagnetism.

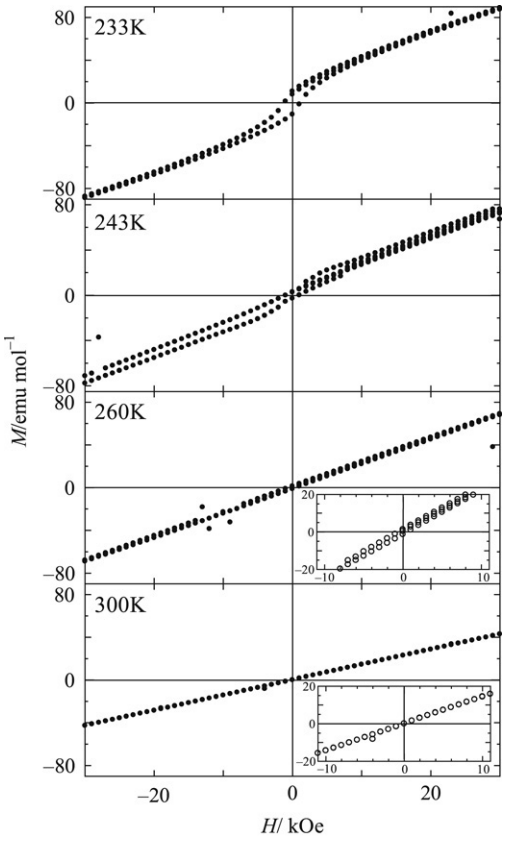

Fig. 2. Magnified $M-H$ curves of $La_{0.87}Sr_{0.13}CrO_3$ at the temperatures above 233 K. Further magnifications are shown in insets.

With increase of temperature, hysteresis became smaller. The hysteresis apparently disappeared in Fig. 1 at the temperatures between 233 and 260 K, however, those with small M_r and H_c were observed as shown in Fig. 2, which is magnification of Fig. 1. The hysteresis completely disappeared at 300 K, indicating that phase transition from canted antiferromagnetic to paramagnetic occurred below 300 K. Fig. 3(a) shows DSC curve of $La_{0.87}Sr_{0.13}CrO_3$ observed in this study. Endothermic peak, corresponding to the structural phase transition from orthorhombic to rhombohedral which had been already confirmed by the previous study [9], was observed at 226 K. The base line shift, which was identified as magnetic phase transition from canted antiferromagnetic to paramagnetic, was detected at 271 K, showing agreement with disappearance of the hysteresis in $M-H$ curve at 300 K. Three phases observed in the DSC measurement, i.e. canted antiferromagnetic orthorhombic, canted antiferromagnetic rhombohedral and paramagnetic rhombohedral are called phase [I], [II] and [III], respectively, in this paper. Fig. 3(b) and (c) shows dependence of M_r and H_c measured from the data depicted in Figs. 1 and 2 on temperature, respectively. Within the phase [I] and [II], both M_r and H_c decreased with increase of temperature, suggesting that entropy of electronic spin configuration prevailed at high temperature. At the boundary of phase [I] and [II], drastic decrease of M_r and variation of temperature dependence of H_c have been observed, originating from structural phase transition

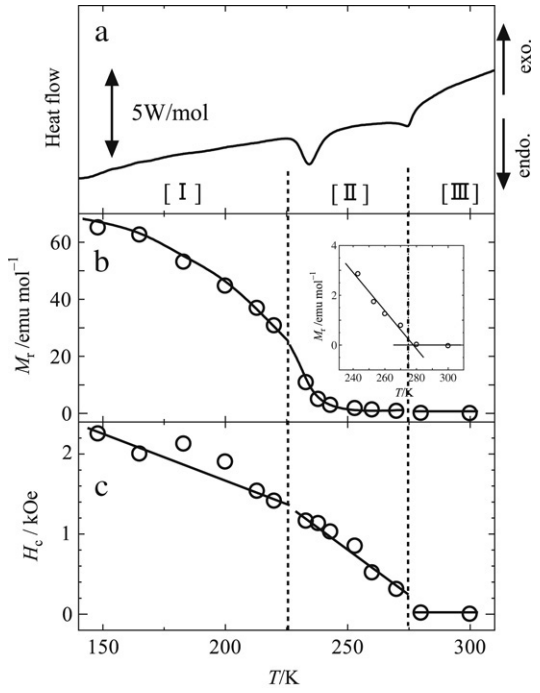

Fig. 3. (a) DSC curve, temperature dependence of (b) residual magnetization, M_r, and (c) coercive force, H_c of $La_{0.87}Sr_{0.13}CrO_3$. Dotted lines represent phase transition temperatures observed by DSC. Inset shows magnetization of temperature dependence of M_r around the second order phase transition.

which will be discussed later. For the paramagnetic phase [III] above 271 K, M_r and H_c should be equal to 0. At the boundary of phase [II] and [III], discontinuity has been observed in both M_r and H_c as inset of Fig. 3(b) shows.

Fig. 4 shows representative $M-H$ curves of $La_{0.85}Sr_{0.15}CrO_3$. Parts of the curves depicted in Fig. 4 were magnified as shown in Fig. 5. The hystereses indicating canted antiferromagnetic property were observed below 250 K. The hysteresis disappeared at 290 K, indicating transition to paramagnetic. However, small deviation from linear relationship was observed, the reason for which has not been identified. Fig. 6 shows (a) DSC curve, (b) variation of M_r on temperature and (c) dependence of H_c on temperature of $La_{0.85}Sr_{0.15}CrO_3$. Although, transition temperatures differ from those of $La_{0.87}Sr_{0.13}CrO_3$, the similar tendency was observed in dependence of M_r and H_c on temperature. Abrupt decrease of M_r and variation of temperature dependence of H_c at the phase boundary between [I] and [II] have also been detected.

4. Discussion

It can be concluded that M_r and H_c of orthorhombic canted antiferromagnetic phase of $La_{1-x}Sr_xCrO_3$ is larger than those of rhombohedral one, indicating that some effects of crystal structure on magnetic property exist. Canted antiferromagnetism of $LaCrO_3$ was explained as follows. Cr in $LaCrO_3$ takes trivalent state with $3d^3$ electronic configuration. In $[CrO_6]$ octahedral in perovskite structure, energy of 3d orbitals splits into two state, one is composed of three kinds of 3d orbitals with lower energy called t_{2g}, the other is composed of two kinds with higher energy, called e_g. The

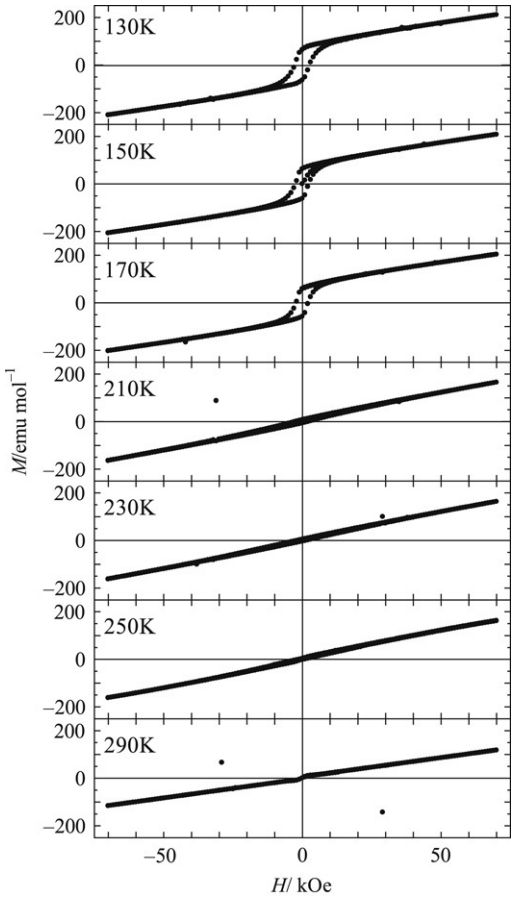

Fig. 4. Dependence of dc magnetization, M, on external magnetic field, H, of $La_{0.85}Sr_{0.15}CrO_3$ at various temperatures.

three 3d electrons in Cr^{3+} occupy t_{2g} state with parallel spin according to Hund's rule and generate large spin on Cr^{3+} ion. If temperature is low enough, superexchange interaction between the large spins on the nearest Cr ions sandwiching O^{2-} ion generates, resulting in antiparallel spin configuration. Since the superexchange interaction is the highest if angle of Cr–O–Cr bond is 180°, hysteresis in M–H curve of $LaCrO_3$ should not be observed if the crystal structure of $LaCrO_3$ was ideal cubic. Due to orthorhombic distortion of $LaCrO_3$ structure, Cr–O–Cr bond angle slightly deviate from 180°, resulting in residual electronic spin originating from imperfect superexchange interaction and hysteresis in M–H curve. Therefore, it can be deduced that higher M_r and H_c can be expected in the phase with large deviation of Cr–O–Cr bond angle from 180°.

It has been already confirmed that the space groups of orthorhombic and rhombohedral $LaCrO_3$ are *Pnma* (No. 62) and $R\bar{3}c$ (No. 167), respectively, by convergent beam electron diffraction [11]. Octahedral tilting and rotational mode of *Pnma* and $R\bar{3}c$ distorted perovskite were analysed by Glazer [12], Woodward [13], Howard and Stocks [14]. They concluded that *Pnma* phase has lower symmetry than that of $R\bar{3}c$ one. Therefore, it can be prospected that distortion of orthorhombic $La_{1-x}Sr_xCrO_3$ phase from ideal perovskite structure is larger than that of rhombohedral phase, resulting in larger deviation of Cr–O–Cr angle from 180° in orthorhombic phase than in rhombohedral one.

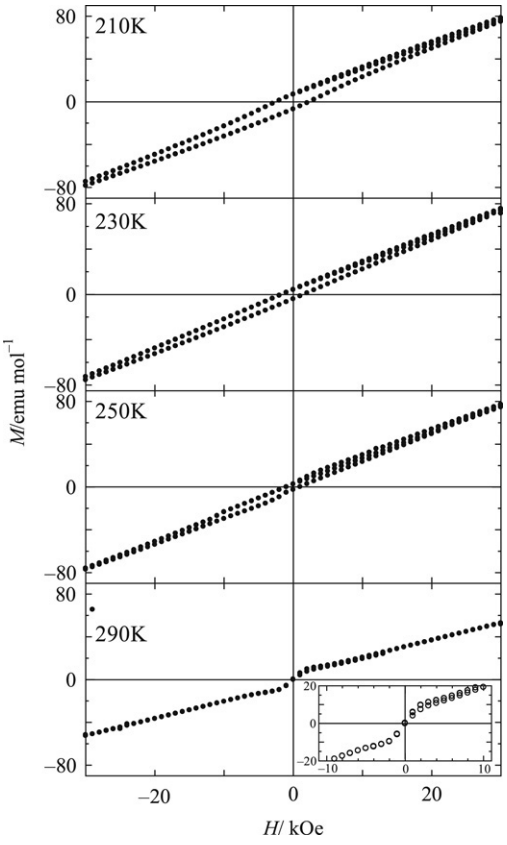

Fig. 5. Magnified M–H curves of $La_{0.85}Sr_{0.15}CrO_3$ at the temperatures above 210 K. Inset shows further magnification of M–H curve at 290 K.

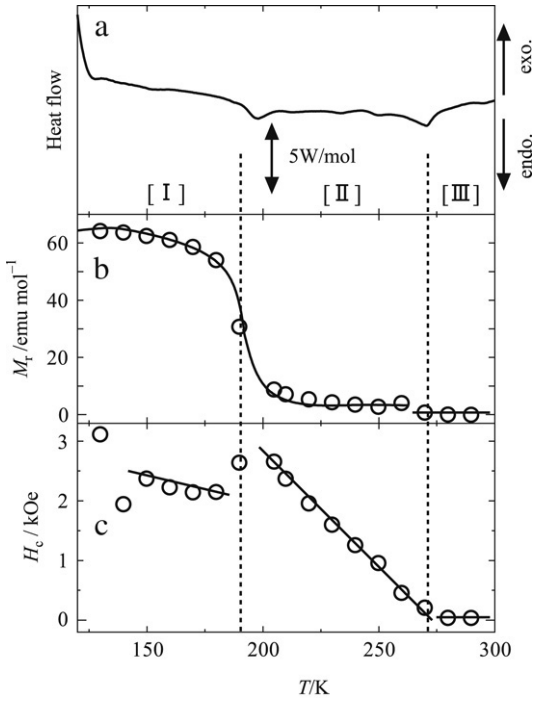

Fig. 6. (a) DSC curve, temperature dependence of (b) residual magnetization, M_r, and (c) coercive force, H_c of $La_{0.85}Sr_{0.15}CrO_3$. Dotted lines represent phase transition temperatures observed by DSC.

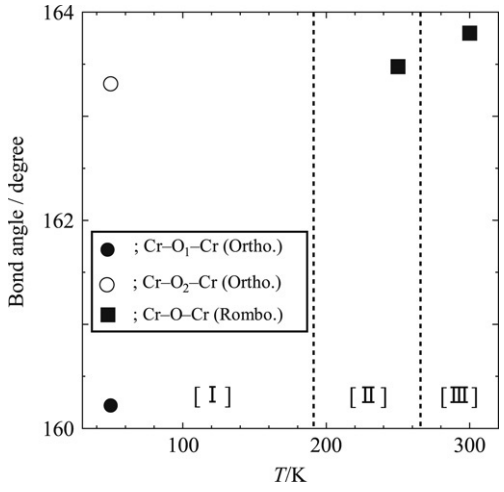

Fig. 7. Cr–O–Cr bond angle of $La_{0.85}Sr_{0.15}CrO_3$ calculated by using atomic parameters obtained by the powder neutron diffraction measurements [8]. Cr–O_1–Cr and Cr–O_2–Cr represent bond parallel and perpendicular to [010], respectively, in orthorhombic *Pnma* phase.

To confirm this prospect experimentally, information on atomic parameter of $La_{0.85}Sr_{0.15}CrO_3$ is necessary, which can be obtained from neutron diffraction measurements. Tezuka and coworkers [8] reported atomic parameters of $La_{0.85}Sr_{0.15}CrO_3$ at 50, 250 and 300 K obtained by neutron diffraction measurements. Fig. 7 shows Cr–O–Cr angles calculated from their reported atomic parameters. In phase [I] with space group of *Pnma*, there are two kinds of Cr–O–Cr bond. One is parallel, the other is perpendicular to [010]. The angles of former and latter Cr–O–Cr bond were 160.22° (depicted as Cr–O_1–Cr in Fig. 7) and 163.31° (depicted as Cr–O_2–Cr in Fig. 7), respectively, at 50 K. In phase [I] and [II] with rhombohedral phase, only one kind of Cr–O–Cr angle is observed. The angles were 163.48° and 163.80° at 250 K and 300 K, respectively. Cr–O–Cr angles depicted in Fig. 7 shows agreement with the prospect that the deviation of Cr–O–Cr angle from 180° is larger in *Pnma* phase than that in $R\bar{3}c$ one. Cr–O–Cr angles in orthorhombic and rhombohedral $LaCrO_3$ estimated by using neutron diffraction were also reported [15]. Since deviation of Cr–O–Cr angle from 180° in rhombohedral $LaCrO_3$ is smaller than that in orthorhombic phase, which was same tendency as $La_{0.85}Sr_{0.15}CrO_3$, it can be expected that this tendency should be also observed regardless of Sr content in $La_{1-x}Sr_xCrO_3$.

The above discussion of crystal structure shows qualitative agreement with larger M_r and H_c in canted antiferromagnetic orthorhombic phase of $La_{1-x}Sr_xCrO_3$ than in rhombohedral one. The abrupt decrease of M_r and variation of temperature dependence of H_c can be qualitatively explained by using the above discussion on crystal structure. In order to quantitative confirmation, direct measurements of Cr–O–Cr angle using neutron diffraction at wide range of temperatures are necessary and they are now in progress.

5. Conclusion

The effect of crystal structure on M–H curves of $La_{1-x}Sr_xCrO_3$ ($x = 0.13$, 0.15) was investigated. At high temperatures, where paramagnetic phase was stable, linear relationships were observed. At low temperatures, where canted antiferomagnatic and orthorhombic-distorted perovskite phase is stable, residual magnetization, M_r, decreased with increase of temperature. At the temperature of the structural phase transition from orthorhombic to rhombohedral, discontinuous decrease of M_r was observed. The dependence of coercive force, H_c, on temperature also varied at the structural phase transition temperature. Larger decrease of H_c on temperature was observed in rhombohedral phase than in orthorhombic phase. We regard that this variation of M_r and H_c could be attributed to difference of deviation of Cr–O–Cr angle from 180° between both structures.

Acknowledgments

Part of this work was supported by the “High-Tech Research Centre” Project for Private Universities and a matching fund subsidy from the Ministry of Education, Culture, Sports, Science and Technology, 2000-2004.

References

[1] N.Q. Minh, J. Amer. Ceram. Soc. 76 (1993) 563.
[2] N. Sakai, H. Fjellvåg, B.C. Hauback, J. Solid State Chem. 121 (1996) 202.
[3] Y. Tokura, A. Urushibara, Y. Moritomo, T. Arima, A. Asamitsu, G. Kido, N. Furukawa, J. Phys. Soc. Japan 63 (1994) 3931.
[4] J. Mizusaki, N. Mori, H. Takai, Y. Yonemura, H. Minamiue, H. Tagawa, M. Dokiya, H. Inaba, K. Naraya, T. Sasamoto, T. Hashimoto, Solid State Ionics 129 (2000) 163.
[5] T. Nakamura, G. Petzow, L.J. Gauckler, Mater. Res. Bull. 14 (1979) 649.
[6] J. Mizusaki, S. Yamauchi, K. Fueki, A. Ishikawa, Solid State Ionics 12 (1987) 119.
[7] S. Onuma, K. Yashiro, S. Miyoshi, A. Kaimai, H. Matsumoto, Y. Nigara, T. Kawada, J. Mizusaki, K. Kawamura, N. Sakai, H. Yokokawa, Solid State Ionics 174 (2004) 287.
[8] K. Tezuka, Y. Hinatsu, A. Nakamura, T. Inami, Y. Shimojo, Y. Morii, J. Solid State Chem. 141 (1998) 404.
[9] F. Nakamura, Y. Matsunaga, N. Ohba, K. Arai, H. Matsubara, H. Takahashi, T. Hashimoto, Thermochim. Acta 435 (2005) 222.
[10] M.P. Pechini, US Patent 330 (3) (1967) 697.
[11] T. Hashimoto, K. Takagi, K. Tsuda, M. Tanaka, K. Yoshida, H. Tagawa, M. Dokiya, J. Electrochem. Soc. 147 (2000) 4408.
[12] A.M. Glazer, Acta Cryst. B 28 (1972) 3384.
[13] P.M. Woodward, Acta Cryst. B 53 (1997) 32.
[14] C.J. Howard, H.T. Stokes, Acta Cryst. B 54 (1998) 782.
[15] K. Oikawa, T. Kamiyama, T. Hashimoto, Y. Shimojo, Y. Morii, J. Solid State Chem. 154 (1998) 524.

Magnetic field effect on the pressure-induced superconducting state in the hole-doped two-leg ladder compound $Sr_2Ca_{12}Cu_{24}O_{41}$

T. Nakanishi,[1,2,*] N. Motoyama,[3,†] H. Mitamura,[1] N. Takeshita,[1,‡] H. Takahashi,[2] H. Eisaki,[3,§] S. Uchida,[3] and N. Môri[1,‖]
[1]*Institute for Solid State Physics, University of Tokyo, 5-1-5 Kashiwanoha, Kashiwa-shi, Chiba 277-8581, Japan*
[2]*College of Humanities and Sciences, Nihon University, 3-25-40 Sakurajosui, Setagaya-ku, Tokyo 156-8550, Japan*
[3]*Department of Superconductivity, University of Tokyo, 2-11-16 Yayoi, Bunkyo-ku, Tokyo 113-8656, Japan*
(Received 16 May 2005; published 24 August 2005)

We report electrical resistivity on a single crystal of the hole-doped two-leg ladder compound $Sr_2Ca_{12}Cu_{24}O_{41}$, which becomes superconducting with $T_c \sim 5$ K only at pressures above ~3.0 GPa. Measurements were performed at nearly hydrostatic pressures up to 5.7 GPa and low temperatures down to 100 mK under static magnetic fields up to 20 T parallel to the *a* axis (along the ladder rungs) and up to 7 T parallel to both the *b* axis (perpendicular to the ladder plane) and the *c* axis (along the ladder legs). A clear difference in the resistive upper critical field $H_{c2}(T)$ is observed among these three directions, confirming that this system has a highly anisotropic superconducting ground state. Also, $H_{c2}(T)$ parallel to the ladder plane is found to exceed the Pauli limit by a factor of more than 2, suggesting either a strong spin-orbit scattering or spin-triplet pairing. Furthermore, it is implied, from measurements of resistivity versus angle of magnetic field in the *bc* plane, that another superconducting phase is stable below around 3 K only when the magnetic field is applied exactly along a certain direction that is ±35° from the ladder direction.

DOI: 10.1103/PhysRevB.72.054520 PACS number(s): 74.62.Fj, 74.72.Jt

I. INTRODUCTION

A concept of $S=\frac{1}{2}$ Heisenberg-type spin-ladder has offered predictions[1–3] of two features: the existence of a spin gap and superconductivity by doped hole-pairs with the spin gap. These are closely related to features of high-T_c cuprates (HTSC). The most important point in the predictions is that the pairing interaction is supposed to be caused by purely electronic origin, namely, magnetic interaction. At present, a compound $Sr_{14-x}Ca_xCu_{24}O_{41}$ (Refs. 4–6) is the only known candidate as a real system having the theoretically predicted properties of the doped spin-ladders as mentioned above, and also is the first nonsquare lattice superconducting cuprate.

This spin-ladder system becomes superconducting with $T_c \lesssim 12$ K only in a pressure P above ~3.0 GPa when $x \geqslant 10$ and the T_c shows the bell-shaped curve against applied pressure.[4–6] These features are quite similar to those of HTSC, having two-dimensional (2D) CuO_2 planes in which the spin gap behavior has been observed so far and the superconducting phase is stabilized only in a certain range of carrier doping. The essential difference is that this ladder system has conducting layers composed by weakly coupled one-dimensional (1D) Cu_2O_3 two-leg ladders with a spin gap and shows 1D charge transport along the ladder at low pressure below ~2 GPa.[7] Furthermore, the anisotropy ratio of the resistivity in this system is quite similar to that of a quasi-1D organic superconductor $(TMTSF)_2PF_6$ (Ref. 8), which has conducting layers composed by weakly coupled 1D chains. On the other hand, the anisotropic electrical resistivity measurements under high pressure[5] indicate that pressure causes a dimensional crossover from 1D to anisotropic 2D charge transport in the normal state and then superconductivity is suggested to occur in the Cu_2O_3 two-leg ladders as in the anisotropic 2D system. However, the superconducting property, especially under magnetic field, of this ladder system is not well understood yet. There are only few measurements concerning the upper critical field on this system, for example, ac susceptibility[9] at a pressure of 4.0 GPa up to 10 T and resistivity[10] at a pressure of 4.8 GPa up to 7 T.

In this paper, we present the results of precise magnetotransport measurements of a $Sr_2Ca_{12}Cu_{24}O_{41}$ single crystal at three different pressures where $dT_c/dP > 0$, $dT_c/dP \simeq 0$, and $dT_c/dP < 0$ in magnetic fields applied along all three crystallographic axes. In these measurements, the magnetic field range is extended up to 20 T parallel to the *a* axis (along the ladder rungs) and up to 7 T parallel to both the *b* axis (perpendicular to the ladder plane) and the *c* axis (along the ladder legs).

II. EXPERIMENT

A single crystal of $Sr_2Ca_{12}Cu_{24}O_{41}$ was grown by the traveling-solvent floating zone method using an infrared furnace under oxygen gas.[7] Using a newly developed self-clamped high-pressure cell[11] that employs Bridgman anvils with a Teflon capsule filled with a pressure transmitting liquid medium (a 1:1 mixture of Fluorinert FC 70 and FC 77), the absolute values of electrical resistivity by a four-probe technique were measured under nearly hydrostatic pressure in the temperature range down to around 100 mK by a dilution refrigerator. A sample with dimensions of 0.3 (*a* axis) $\times 0.2$ (*b* axis) $\times 0.7$ (*c* axis) mm^3 was used in the resistivity measurements with an ac current (10 or 100 μA at 15.9 Hz, ohmic response without self-heating effect was confirmed within this current range) along the *c* axis. We used two superconducting magnets: a Helmholtz-type horizontal rotatable 7 T parallel to the *bc* plane and a cylindrical 20 T parallel to the *a* axis. Although it was required to warm the cryostat with the pressure cell up to around 100 K in order to

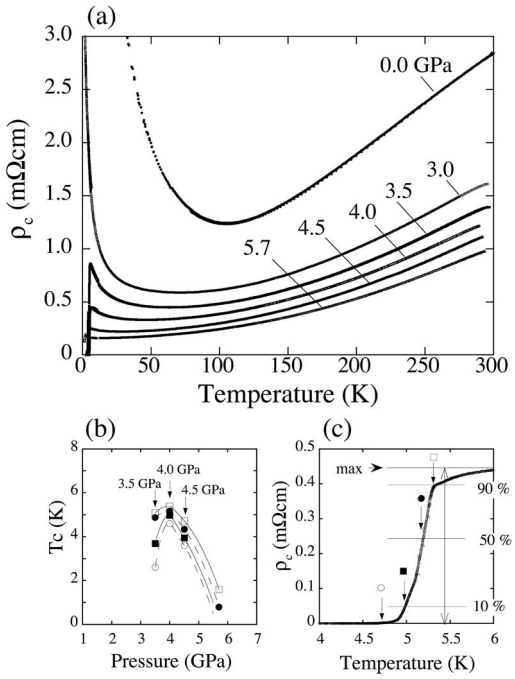

FIG. 1. (a) $\rho_c(T)$ of $Sr_2Ca_{12}Cu_{24}O_{41}$ at several pressures. (b) Pressure dependence of T_c that was determined by several criteria as illustrated in (c) for the case at 4.0 GPa as an example where we define T_c, which satisfies a condition that $\rho_c(T_c)$ is equal to a fixed percentage of the resistive maximal value before the transition. Lines in (b) are guides for the eyes.

change a magnet to another at a fixed pressure, this thermal cycle did not cause any change in the pressure because T_c did not change in this process. This ensured that these experiments were done under exactly the same pressures for the identical sample.

For pressure calibration at low temperatures in this pressure cell, we have measured the temperature dependence of ac susceptibility of lead to determine the superconducting transition temperature. In this measurement, at ambient pressure, the superconducting transition temperature T_c is observed at 7.2 K, with a transition width ΔT_c of 0.03 K. It is noted that the ΔT_c under each pressure still remains 0.03 K, which is at ambient pressure. This result clearly indicates that the generated pressures in this pressure cell are close to the hydrostatic one although the pressure transmitting medium is solidified in this temperature region. From this result, we construct the pressure calibration curve of this pressure cell by using the data of Bireckoven and Wittig.[12] A reproducibility of this curve is confirmed with a precision of ±0.1 GPa at 2.55 GPa by four different measurements which monitor the resistive transition of Bi due to the I-II structural phase transition at room temperature. More detailes are described elsewhere.[11]

III. RESULTS AND DISCUSSION

A. ρ_c under magnetic fields

Figure 1(a) shows the temperature dependence of resistivity ρ_c along the c axis of $Sr_2Ca_{12}Cu_{24}O_{41}$ up to 5.7 GPa. At ambient pressure, ρ_c is ~3 mΩ cm at room temperature and shows T-linear metallic dependences upon cooling. These facts indicate that this ρ_c clearly shows the transport properties of the c axis, namely, the ladder direction at ambient pressure. At room temperature, ρ_c decreases with pressure continuously. Above 3.5 GPa the sample becomes superconducting at around 5 K and the T_c exhibits the bell-shaped curve against pressure as shown in Fig. 1(b) where T_c is determined in several ways as shown in Fig. 1(c). These pressure effects on the transport and superconducting properties in the zero field are consistent with the previously reported results on the $x=11.5$ single crystal.[5]

Figure 2 shows the temperature dependence of ρ_c of $Sr_2Ca_{12}Cu_{24}O_{41}$ at 3.5, 4.0, and 4.5 GPa in various magnetic fields applied along the a axis up to 20 T and the b axis up to 7 T. It is clearly observed that, with increasing pressure from 3.5 to 4.5 GPa, the pressure influences the qualitative changes in the behavior of resistive-transition in the magnetic fields. For the fields up to 7 T along the b axis, at 3.5 and 4.0 GPa the superconductivity is not completely destroyed while at 4.5 GPa $\rho_c(T)$ at 5.5 and 7 T shows almost the same curve at least down to around 1 K. These qualitative changes in the behavior of resistive transition in the magnetic fields are also observed in field sweep measurements at fixed temperatures. The results are shown in Fig. 3, where the fields were applied along the a axis up to 18 T and the b axis up to 7 T at pressures of 4.0 and 4.5 GPa. As seen in Fig. 3, for the fields up to 7 T along the b axis, at 4.0 GPa the resistivity has not reached a constant value while at 4.5 GPa the resistivity has reached a constant value at 7 T. These facts indicate that normal state resistivity is recovered at 4.5 GPa under the magnetic fields along the b axis above 5.5 T at temperatures down to about 1 K. Thus the $\rho_c(T)$ curve at 4.5 GPa above 1 K under 7 T along the b axis refers to normal state resistivity.

B. Resistive upper critical field

The resistive upper critical field $H_{c2}(T)$ is defined as the magnetic field where the normal state resistivity is recovered in the measurement of field sweep at a fixed temperature. In this sense, we can determine $H_{c2}(T)$ only for data at 4.5 GPa where the normal state resistivity is recovered within the measured magnetic field range. However, due to the difficulty of applying this criterion to the data perfectly, we determined critical magnetic fields H^n where $\rho_c(T)$ is equal to a fixed percentage ($n=10\%$, 50%, and 90% and $n=$"$\rho=0$" for 0%) of the normal state resistivity, that is $\rho_c(T)$ curve above 1 K at 4.5 GPa and 7 T as denoted $\rho_c(H=7\mathrm{T}//b)$ as shown in Fig. 4. From the field dependence of the resistive transition as shown in Figs. 2 and 3, together with the results along the c axis not shown here, the critical fields at 4.5 GPa for all crystallographic axes are determined and summarized in Fig. 5. Figure 6 shows a summary of critical fields $H^{\rho=0}$ at several pressures. As we can see in Figs. 5 and 6, it is found that there is no significant discrepancy between the results from temperature sweep and field sweep data. Also, it is noted that $H_{c2}(T) > H^{90\%}(T)$ and $H^{\rho=0}(T)$ corresponds to the irreversibility line in the case of HTSC. As it has been observed and

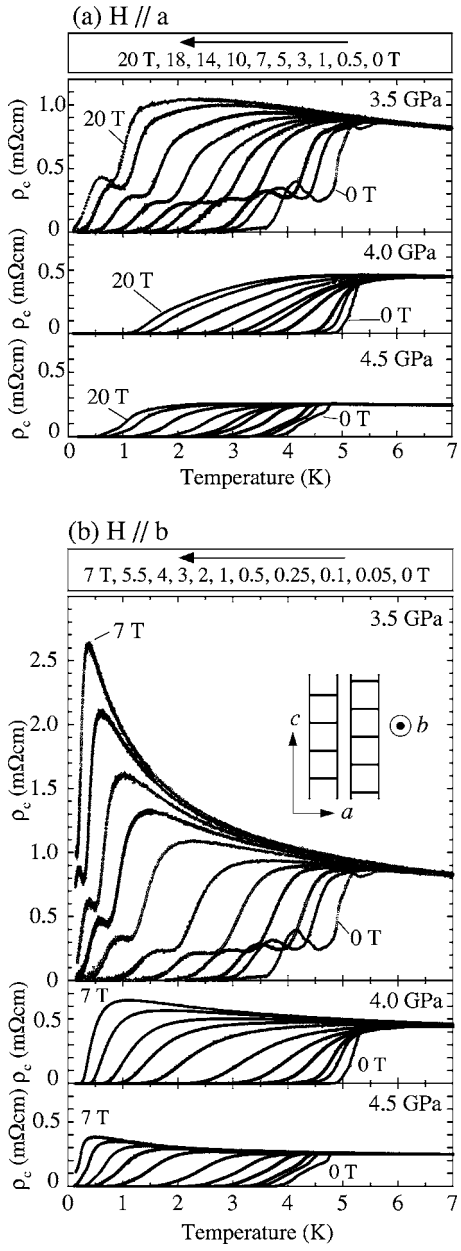

FIG. 2. $\rho_c(T)$ of $Sr_2Ca_{12}Cu_{24}O_{41}$ at 3.5, 4.0, and 4.5 GPa in various magnetic fields along (a) the *a* axis and (b) the *b* axis. Inset in (b) shows a schematic structure of the two-leg ladders viewed from the *b* axis.

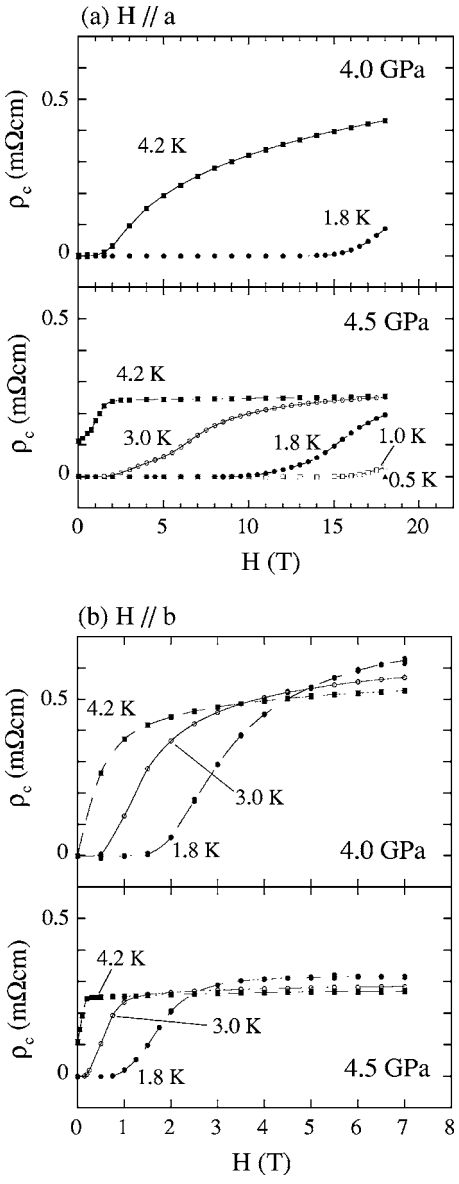

FIG. 3. Magnetic field dependence of ρ_c of $Sr_2Ca_{12}Cu_{24}O_{41}$ at 4.0 and 4.5 GPa and at several temperatures for the fields along (a) the *a* axis and (b) the *b* axis.

discussed in HTSC, it is difficult to interpret the resistive upper critical field because in some cases the motion of flux may affect the shape of the resistive transition. However, at present we cannot distinguish a difference between the resistive upper critical field and the thermodynamic upper critical field for the present ladder system because of the technical difficulty of performing thermodynamic experiments, such as specific heat, at hydrostatic pressures above 3 GPa under magnetic fields.

As observed in Fig. 5, there is the clear difference in the critical fields, also implied in $H_{c2}(T)$ as well, among these three directions. This fact clearly indicates that this system has a highly anisotropic superconducting ground state. It is seen in Fig. 6 that the anisotropy of $H^{\rho=0}(T)$ is unchanged at three different pressures where $dT_c/dP>0$, $dT_c/dP\simeq 0$, and $dT_c/dP<0$ within measured temperature and magnetic field range, implying that the anisotropy of $H_{c2}(T)$ is also unchanged in the whole pressure range. The most important fact seen in Fig. 5 is that H_{c2} along the *a* axis, parallel to the conducting ladder plane, exceeds the value of Pauli paramagnetic limit [as indicated by arrows in Fig. 5 for a criterion of $T_c(50\%)$] by a factor of more than 2, which is given by $H_p(T=0)=1.84\ T_c(H=0)$ for isotropic singlet *s*-wave pairing without spin-orbit scattering.[13]

As reported by the anisotropic electrical resistivity measurements under high pressure,[5] superconductivity is suggested to occur in the Cu_2O_3 two-leg ladders as in the anisotropic 2D system. This implies that coherence length along the *b* axis ξ_b becomes shorter than a distance between the

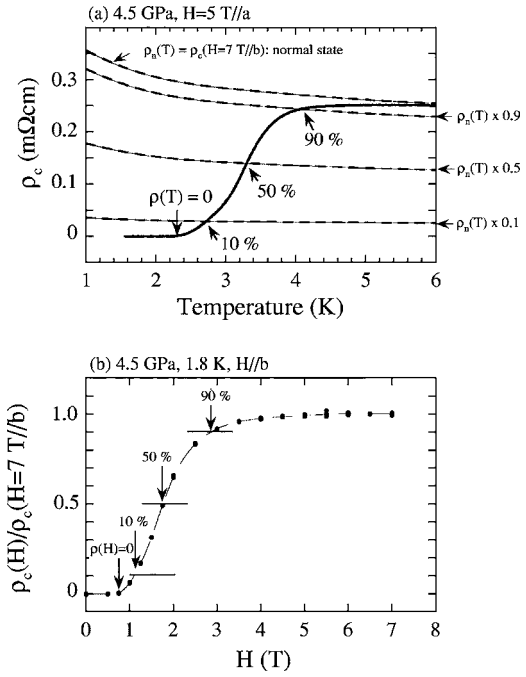

FIG. 4. Examples of criteria to define T_c, where we define T_c which satisfies a condition that $\rho_c(T_c, H^n)$ is equal to a fixed percentage n of the normal state value $\rho_n = \rho_c(H=7\ \mathrm{T}\|b)$ at 4.5 GPa for (a) the temperature sweep data and for (b) the field sweep data.

ladder plane. In fact, a value of $\rho_c \sim 0.5\ \mathrm{m\Omega\,cm}$ gives a mean free path along the c axis $l_c \sim 10-100$ Å by assuming a simple free electron model with a carrier density estimated from a Hall coefficient of $\sim 2\times 10^{-3}\ \mathrm{cm^3/C}$.[14] We would

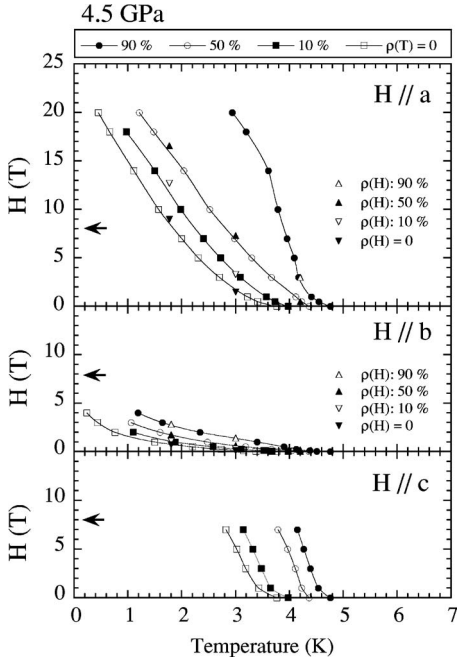

FIG. 5. Critical fields $H^{90\%}$, $H^{50\%}$, $H^{10\%}$, $H^{\rho=0}$ of $Sr_2Ca_{12}Cu_{24}O_{41}$ at 4.5 GPa for H$\|a$ axis, H$\|b$ axis, and H$\|c$ axis. Data for $\rho_c(H)$: 90%, 50%, and 10% and $\rho_c(H)=0$ are from the field sweep data (Fig. 3). Lines are guides for the eyes. Arrows indicate $H_p(T=0)$ for $T_c(50\%)$ (see text).

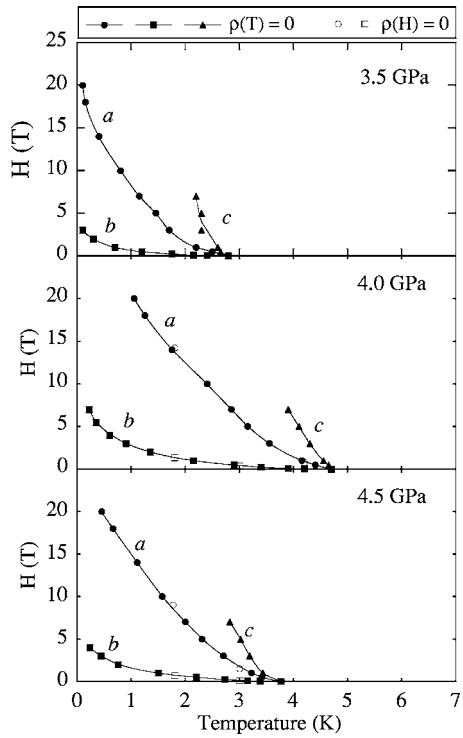

FIG. 6. Critical fields $H^{\rho=0}$ at 3.5, 4.0, and 4.5 GPa for H$\|a$ axis, H$\|b$ axis, and H$\|c$ axis. Lines are guides for the eyes.

expect ρ_b to be lower than ρ_c by two orders of magnitude,[7] this means l_b to be $\sim 0.1-1$ Å. Also, this system is supposed to be a dirty superconductor due to being a highly doped system; thus we expect that coherence length ξ is shorter than l; then ξ_b would be less than $\sim 0.1-1$ Å. This fact implies that ξ_b seems to be shorter than the distance between the ladder planes about 7 Å.[15] Therefore ξ_b is expected to become smaller than the ladder spacing at a certain temperature. Below this temperature orbital effects as a mechanism for the quenching of superconductivity might be suppressed, then H_{c2} parallel to the ladder plane would be infinite in the absence of both Pauli limit and spin-orbit scattering that reduces Pauli paramagnetic effect, as predicted for the upward curvature of $H_{c2}(T)$ for 2D layered superconductors.[16] Thus one possible explanation for the observed absence of Pauli limit is that there is a spin-orbit scattering that is strong enough for the quenching Pauli paramagnetic effect, as observed in layered superconductors $TaS_{2-x}Se_x$ ($x=0$ and 0.4).[17] Besides such a strong spin-orbit scattering, one may speculate that another possible explanation for the absence of Pauli limit might be due to spin-triplet pairing. In fact, very recently, Fujiwara *et al.*[18] have shown, from the high-pressure NMR experiment at 3.5 GPa, that the Knight shift does not change at T_c within their experimental accuracy. This fact indicates a possibility of triplet superconductivity in this system. Furthermore, they have also observed the peak of T_1^{-1} at T_c. These behaviors are quite similar to those of a quasi-1D molecular superconductor $(TMTSF)_2PF_6$ in which a large evolution of H_{c2} parallel to conducting layers at low temperatures, exceeding the Pauli limit, has been observed.[19] This might be due to spin-triplet pairing that has been shown recently.[20] In contrast, the Pauli limit is observed

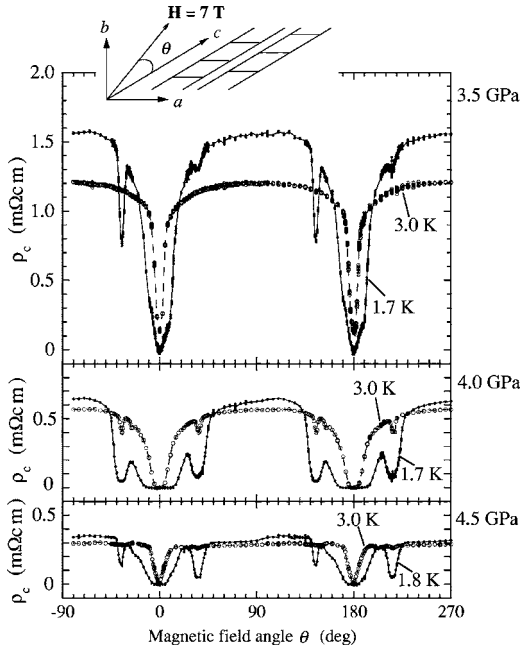

FIG. 7. ρ_c vs angle θ of a magnetic field $H=7$ T in the bc plane of $Sr_2Ca_{12}Cu_{24}O_{41}$ at pressures of 3.5, 4.0, and 4.5 GPa in the two different temperature regions of 1.7 to 1.8 (open circles) and 3 K (closed circles). Lines are guides for the eyes.

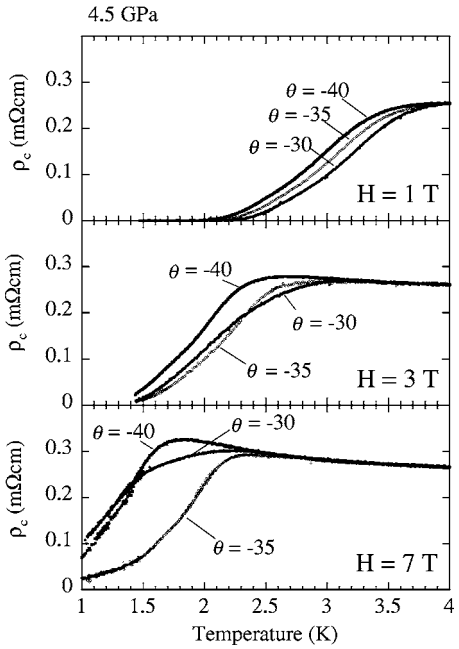

FIG. 8. $\rho_c(T)$ of $Sr_2Ca_{12}Cu_{24}O_{41}$ in fields $H=1$, 3, and 7 T in the bc plane with angles of $\theta=-30°$, $-35°$, and $-40°$ from c axis (ladder direction).

in $YBa_2Cu_3O_{7-\delta}$ (Ref. 21) for H_{c2} parallel to the conducting CuO_2 layer, in which a singlet d-wave superconducting state might be realized.

C. ρ_c vs angle of magnetic field in the bc plane

Figure 7 shows the results of ρ_c versus angle of magnetic field of 7 T in the bc plane in the two different temperature regions, 1.7 to 1.8 K and 3.0 K, at each pressure. As seen in the figure, apart from resistive drops at the ladder direction (c axis: $\theta=0°$ and 180°) due to the anisotropy of the critical field, other extra resistive drops are clearly observed at the angles of ±35° from the ladder direction symmetrically. This angle is independent of both current and magnetic field, which indicates that these resistive drops are not caused by the motion of flux due to the Lorentz force, which depends on both current and magnetic field. The angle is also independent of applied pressure. On the other hand, the sharpness of this resistive drops at ±35° seems to be similar to that at c axis, namely, $\theta=0$ and 180°. Therefore this resistive anomaly is supposed to be caused by superconductivity, possibly another superconducting phase. Also, it is difficult to explain that the symmetrical appearance of this additional superconducting phase at the angles of ±35° from the ladder direction would be caused by the inhomogeneity of a pressure-induced superconducting region in the sample. Figure 8 shows the results of $\rho_c(T)$ curves at 4.5 GPa under three different magnetic fields, 1, 3, and 7 T, applied along the directions with three different angles of −30°, −35°, and −40° from the ladder direction. At 1 T the shift of resistive transition in these curves seems to be in accordance with its anisotropy from −30° to −40°. With increasing fields, the shift of the transition goes to lower temperature; then, just after passing through around 2 to 3 K, the shift of the transition in the curve with an angle of −35° starts to deviate from the two curves with angles of −30° and −40°. This behavior is also observed in field sweep measurements at 1.8 K with different field angles, as shown in Fig. 9. These facts indicate that this additional superconducting phase becomes to develop below around 3 K only when the magnetic field is applied exactly along a certain direction that is ±35° from the ladder direction. Although, at present, a physical meaning of ±35° from the ladder direction is unknown, we might say at least that the appearance of this additional superconducting phase clearly depends on both the temperature and the direction of the applied magnetic field. Also, it is noted that this addi-

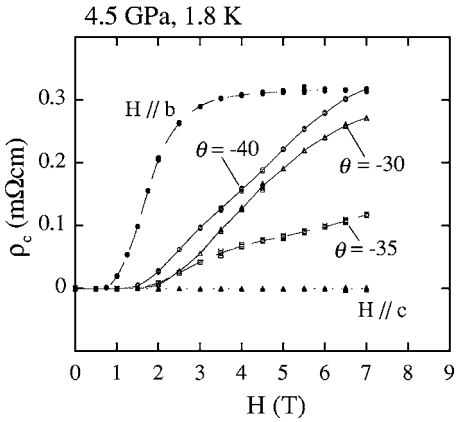

FIG. 9. Magnetic field dependence of $\rho_c(H)$ of $Sr_2Ca_{12}Cu_{24}O_{41}$ at 4.5 GPa and 1.8 K for the fields in the bc plane with angles of $\theta=-30°$, $-35°$, $-40°$, 90° ($H\|b$), and 0° ($H\|c$). Lines are guides for the eyes.

tional superconducting phase appears at three different pressures. Additionally, we would like to point out a possibility that a physical meaning of ±35° is related to a mathematical relation: $\tan^{-1}(\frac{7}{10})=34.99°$. However, in order to confirm whether or not the additional superconducting phase exists in the pressure-induced superconducting state in the $Sr_2Ca_{12}Cu_{24}O_{41}$, precise specific heat measurements at pressures above 3 GPa under magnetic fields are required for future study.

IV. CONCLUSION

In summary, we report the results of precise magnetotransport measurements of a hole-doped two-leg ladder $Sr_2Ca_{12}Cu_{24}O_{41}$ single crystal in fields applied along all three crystallographic axes. The clear difference in the resistive upper critical field $H_{c2}(T)$ is observed among these three directions, indicating that this system has a highly anisotropic superconducting ground state. Also, the absence of Pauli limit in H_{c2} parallel to the conducting ladder plane is found, which suggests either a strong spin-orbit scattering or spin-triplet pairing. Furthermore, it is implied, from measurements of resistivity versus angle of magnetic field in the *bc* plane, that an additional superconducting phase is stable below around 3 K only when the magnetic field is applied exactly along a certain direction that is ±35° from the ladder direction.

ACKNOWLEDGMENTS

We thank T. Nagata and J. Akimitsu for their collaboration in the early stage of this study. One of us (T.N.) would also like to thank G. Sparn and F. Steglich for their kind hospitality during his preparing the manuscript. This work was supported by a Grant-in-Aid for Scientific Research from the Japanese Ministry of Education, Culture, Sports, Science and Technology.

*Present address: Max Planck Institute for Chemical Physics of Solids, Nöthnitzer Strasse 40, D-01187 Dresden, Germany. Electronic address: tks@cpfs.mpg.de

†Present address: Department of Physics, Aoyama-Gakuin University, 5-10-1 Fuchinobe, Sagamihara-shi, Kanagawa 229-8558, Japan.

‡Present address: Joint Research Center for Atom Technology, 1-1-4 Higashi, Tsukuba-shi, Ibaraki 304-0046, Japan.

§Present address: Nanoelectronic Research Institute, AIST, 1-1-1 Umezono, Tsukuba 305-8568, Japan.

‖Present address: Department of Physics, Saitama University, 255 Shimookubo, Saitama-shi, Saitama 338-8570, Japan.

[1] E. Dagotto, J. Riera, and D. Scalapino, Phys. Rev. B **45**, 5744 (1992).

[2] T. M. Rice, S. Gopalan, and M. Sigrist, Europhys. Lett. **23**, 445 (1993).

[3] E. Dagotto, Rep. Prog. Phys. **62**, 1525 (1999).

[4] M. Uehara, T. Nagata, J. Akimitsu, H. Takahashi, N. Môri, and K. Kinoshita, J. Phys. Soc. Jpn. **65**, 2764 (1996).

[5] T. Nagata, M. Uehara, J. Goto, J. Akimitsu, N. Motoyama, H. Eisaki, S. Uchida, H. Takahashi, T. Nakanishi, and N. Môri, Phys. Rev. Lett. **81**, 1090 (1998).

[6] N. Motoyama, H. Eisaki, S. Uchida, N. Takeshita, N. Môri, T. Nakanishi, and H. Takahashi, Europhys. Lett. **58**, 758 (2002).

[7] N. Motoyama, T. Osafune, T. Kakeshita, H. Eisaki, and S. Uchida, Phys. Rev. B **55**, R3386 (1997).

[8] C. S. Jacobsen, K. Mortensen, M. Weger, and K. Bechgaard, Solid State Commun. **38**, 423 (1981).

[9] T. Nakanishi, H. Takahashi, N. Takeshita, N. Môri, N. Motoyama, H. Eisaki, S. Uchida, H. Fujino, T. Nagata, and J. Akimitsu, Physica B **281&282**, 957 (2000).

[10] D. Braithwaite, T. Nagata, I. Sheikin, H. Fujino, J. Akimitsu, and J. Flouquet, Solid State Commun. **114**, 533 (2000).

[11] T. Nakanishi, N. Takeshita, and N. Môri, Rev. Sci. Instrum. **73**, 1828 (2002).

[12] B. Bireckoven and J. Wittig, J. Phys. E **21**, 841 (1988).

[13] A. M. Clogston, Phys. Rev. Lett. **9**, 266 (1962); B. S. Chandrasekar, Appl. Phys. Lett. **1**, 7 (1962).

[14] T. Nakanishi, N. Môri, C. Murayama, H. Takahashi, T. Nagata, M. Uehara, J. Akimitsu, K. Kinoshita, N. Motoyama, H. Eisaki, and S. Uchida, J. Phys. Soc. Jpn. **67**, 2408 (1998).

[15] M. Isobe, M. Onoda, T. Ohta, F. Izumi, K. Kimoto, E. Takayama-Muromachi, A. W. Hewat, and K. Ohoyama, Phys. Rev. B **62**, 11667 (2000).

[16] R. A. Klemm, A. Luther, and M. R. Beasley, Phys. Rev. B **12**, 877 (1975).

[17] D. E. Prober, R. E. Schwall, and M. R. Beasley, Phys. Rev. B **21**, 2717 (1980).

[18] N. Fujiwara, N. Môri, Y. Uwatoko, T. Matsumoto, N. Motoyama, and S. Uchida, Phys. Rev. Lett. **90**, 137001 (2003).

[19] I. J. Lee, M. J. Naughton, G. M. Danner, and P. M. Chaikin, Phys. Rev. Lett. **78**, 3555 (1997).

[20] I. J. Lee, S. E. Brown, W. G. Clark, M. J. Strouse, M. J. Naughton, W. Kang, and P. M. Chaikin, Phys. Rev. Lett. **88**, 017004 (2002).

[21] J. L. O'Brien, H. Nakagawa, A. S. Dzurak, R. G. Clark, B. E. Kane, N. E. Lumpkin, R. P. Starrett, N. Miura, E. E. Mitchell, J. D. Goettee, D. G. Rickel, and J. S. Brooks, Phys. Rev. B **61**, 1584 (2000).

Available online at www.sciencedirect.com
ScienceDirect
Journal of Physics and Chemistry of Solids 69 (2008) 358–361
JOURNAL OF PHYSICS AND CHEMISTRY OF SOLIDS
www.elsevier.com/locate/jpcs

Optical properties of $Sr_{1-x}Eu_xGa_2S_4$ mixed compounds

Chiharu Hidaka, Takeo Takizawa*

Department of Physics, College of Humanities and Sciences, Nihon University, Sakura-josui 3-25-40, Setagaya-ku, Tokyo 1568550, Japan

Abstract

The mixed crystal system of $CaGa_2S_4$–$EuGa_2S_4$ has already been investigated and confirmed to form the solid solution. In this report, the same procedure of the previous report is applied to the $SrGa_2S_4$–$EuGa_2S_4$ system using differential thermal analysis and X-ray diffraction. It is shown that the solid solution is also formed in this system. Photoluminescence spectra of the present system have a broad-wavelength peak characteristic of the phonon-terminated 5d–4f transitions. The peak energy of the emission shifts to the low-energy side as x increases. The maximum intensity of the emission is attained at 10 mol% as about four times larger in magnitude than the emission of a stoichiometric $EuGa_2S_4$ compound.

Keywords: A. Inorganic compounds; B. Chemical synthesis; D. Luminescence; D. Optical properties

1. Introduction

Alkaline earth thiogallates (MGa_2S_4, M = Ca, Sr, Ba) doped with Ce^{3+} and Eu^{2+} exhibit broad emissions due to the phonon-terminated transition between 5d and 4f levels [1]. As the emissions show high luminance in the blue to yellow region, the compounds are expected to be used in display and lighting applications. Many works concerning electroluminescence devices and light emission diodes have been reported [2–6].

Moreover, laser action was observed in Dy^{3+} or Eu^{2+}-doped $CaGa_2S_4$ [7,8]. Thus, the compounds above are also attractive as host crystals of laser materials. Especially, the broad emission arising from the 5d–4f transition may allow us to use Sr- and Ca-thiogallates doped with Ce^{3+} and Eu^{2+} to realize for tunable laser devices in the visible region. At present, the photoluminescence (PL) quantum efficiency of $CaGa_2S_4$:Eu^{2+} (1 at%) was estimated to be 30% [9]. On the other hand, that of a stoichiometric compound of $EuGa_2S_4$ in which all Ca atoms were substituted by the Eu atoms was obtained as 21% [10]. This suggests that a $Ca_{1-x}Eu_xGa_2S_4$ compound with an appropriate composition may have the maximum PL quantum efficiency. Until now, we have studied the single crystal growth and optical properties of $Ca_{1-x}Eu_xGa_2S_4$ ($x = 0$–1) toward the realization of a laser [11]. And we have reported that $Ca_{1-x}Eu_xGa_2S_4$ compounds form the solid solution and the PL intensity had maximum at $x = 0.25$.

Here, we focus our attention on the Sr thiogallate, i.e., $Sr_{1-x}Eu_xGa_2S_4$ to find the best value of x for PL, since the compound has been known as an excellent green phosphor with good purity of color and high brightness [1]. Peter and Baglio briefly described in their paper that $Sr_{1-x}Eu_xGa_2S_4$ compounds formed the solid solution [1]. However, experimental data as well as optical properties concerning these facts have not been reported.

$EuGa_2S_4$ compounds also have the same crystal structure as that of $SrGa_2S_4$, leading us to expect that the Sr ions can be substituted by the Eu ions at any amount in $Sr_{1-x}Eu_xGa_2S_4$. The maximum quantum efficiency is also expected at an appropriate x in the chemical formula above. In this work, we report on the solid solution in the $SrGa_2S_4$–$EuGa_2S_4$ system in terms of the differential thermal analysis (DTA) and powder X-ray diffraction. We discuss the PL and PL excitation (PLE) spectra of the compounds along with the related levels of Eu^{2+} ions in the mixed compound.

*Corresponding author. Tel./fax: +81 3 5317 9772.
E-mail address: takiz@chs.nihon-u.ac.jp (T. Takizawa).

0022-3697/$ - see front matter © 2007 Elsevier Ltd. All rights reserved.
doi:10.1016/j.jpcs.2007.07.016

2. Phase diagram of the $SrGa_2S_4$–$EuGa_2S_4$ system

To investigate the phase diagram of the $SrGa_2S_4$–$EuGa_2S_4$ system, DTA was performed. Compounds of SrS, EuS and Ga_2S_3 were weighed to about 0.3 g in total in Ar atmosphere at an appropriate composition of $Sr_{1-x}Eu_xGa_2S_4$ ($0 \leqslant x \leqslant 1$). These compounds were evacuated in a quartz ampoule of $7\,mm^{\Phi} \times 40\,mm$ for DTA measurements. DTA curves were obtained at a speed of 2 °C/min by scanning twice; whole of the chemical reaction was completed in the first scan and the compounds with the value of x were synthesized. The transition and melting points can be determined in the second scan. In the cooling process of DTA, the supercooling sometimes occurred, where the solidifying points were not determined.

After DTA measurements, powder X-ray diffraction patterns were measured at 300 K by using the CuKα line (40 kV, 30 mA). A single phase of the orthorhombic structure belonging to D_h^{24}-Fddd was found. As Eu concentration increases, diffraction lines shift to the high diffraction angle. The lattice parameters of $SrGa_2S_4$ and $EuGa_2S_4$ are calculated as 20.85, 20.51, 12.22 Å and 20.73, 20.41, 12.20 Å, respectively. These values are compared with the reported data [1]. In the composition of $0 \leqslant x \leqslant 1$, the a- and b-axes decrease and the c-axis stays constant as x increases. Based on the results of DTA and XRD measurements, the phase diagram of the $SrGa_2S_4$–$EuGa_2S_4$ system is shown in Fig. 1. It is considered that the solid solution was formed in the $SrGa_2S_4$–$EuGa_2S_4$ system. This assures that a compound of $Sr_{1-x}Eu_xGa_2S_4$ can be prepared at any x.

3. PL spectra of $Sr_{1-x}Eu_xGa_2S_4$

PL spectra were measured using a spectrometer equipped with a CCD detector (HAMAMATSU, PMA11) at room temperature. A He–Cd laser (325 nm) was used as an excitation light source. The products after DTA measurements were used for the measurements. The products were ground and filled in a quartz tube of $3\,mm^{\Phi} \times 30\,mm$.

The PL spectra of $Sr_{1-x}Eu_xGa_2S_4$ ($0 < x \leqslant 1$) were shown in Fig. 2. The spectra were similar to those of Eu^{2+}-doped $SrGa_2S_4$ and understood as due to the 5d–4f transition of Eu^{2+} ions [1,4]. Fig. 3 shows the integrated PL intensity as a function of Eu concentration. The emission intensity has the maximum value at 10 mol% ($x = 0.1$). The reduction in PL intensity above this value is due to the so-called concentration quenching. The energy of emission peak shifts to the lower energy side with increasing Eu concentration. The ionic radii of Sr and Eu are 1.26 and 1.25 Å, respectively [12]. The lattice volume decreases with increasing Eu concentration x. Thus when Eu concentration continuously increases, the crystal field around a Eu ion becomes stronger as the number of the surrounding

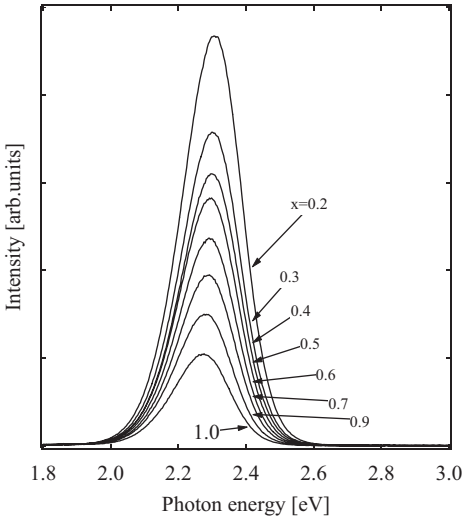

Fig. 2. Photoluminescence spectra of $Sr_{1-x}Eu_xGa_2S_4$ ($0 \leqslant x \leqslant 1$) at 300 K. The emissions are due to 5d–4f transition of Eu^{2+} ions.

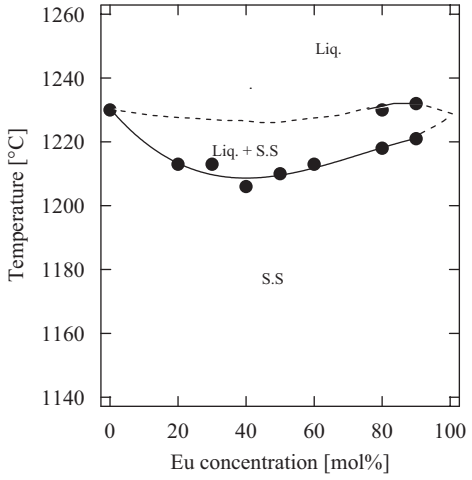

Fig. 1. Phase diagram of the $SrGa_2S_4$–$EuGa_2S_4$ system. Solid solution (S.S) is formed in the Eu concentration between 0 and 100 mol%.

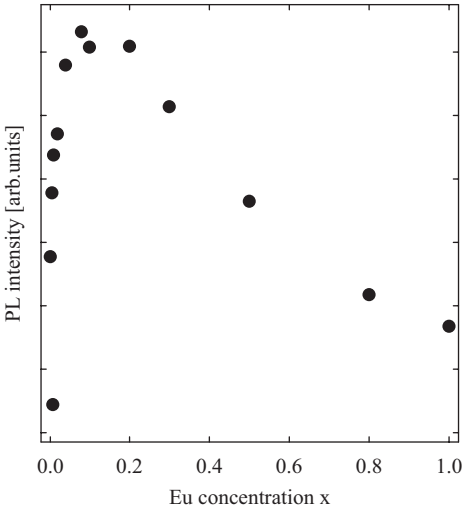

Fig. 3. The PL integrated intensity as a function of Eu concentration. The maximum intensity is obtained at 10 mol%($x = 0.1$).

ions increases. Then, the split of excited states of 5d levels broadens and the energy difference between the lowest excited state of 5d levels and 4f levels decreases.

4. PLE spectra

PLE spectra were measured at 300 K. A xenon lamp of 300 W together with a monochromator (Bunkoh-Keiki SM-25) was used as a light source. PLE was detected by monitoring at 2.3 eV with a photomultiplier (HAMAMATSU, R562) and a monochromator (Nikon, G250). Powdered samples as previously mentioned were used. Fig. 4 shows the PLE spectra of $Sr_{1-x}Eu_xGa_2S_4$ ($x = 0.01$, 0.1, 0.5, 1). The spectra were normalized at 2.5 eV. In a low Eu concentration, three excited levels are found at 2.5, 3.1 and 3.8 eV. The Sr atoms in $SrGa_2S_4$ are surrounded by eight sulfur atoms forming a square anti-prism. When the compound was doped with Eu, the Sr atoms are substituted by the Eu atoms and the Eu atoms are exposed to the crystal field of the D_{4d} symmetry. The 5d states of the Eu ions are splitz into three levels corresponding to the values obtained in the excitation spectra.

5. Energy levels of Eu in $Sr_{1-x}Eu_xGa_2S_4$

An energy diagram of Eu^{2+} in $SrGa_2S_4$ was reported by Chartier et al. [13]. Fig. 5 shows the energy levels of Eu^{2+} in $Sr_{1-x}Eu_xGa_2S_4$. The value of E_{vc} for $SrGa_2S_4$ can be estimated as 4.4 eV from the optical band gap of $CaGa_2S_4$ (4.2 eV) [14]. The 4f state of Eu^{2+} locates at 1.75 eV from the valence band [15]. Thus from the peak energy of PLE, the difference between the lowest 5d level and the 4f level was determined to be 2.5 eV. As a result, the middle and highest levels of the 5d states locates within the conduction band. From PLE, the peaks at 3.1 and 3.8 eV decreased and became blurred with increasing Eu concentration. It is considered that the band structure changes with increasing Eu concentration. When the number of the Eu atoms in $Sr_{1-x}Eu_xGa_2S_4$ increases, the d-band of Eu^{2+} ions gradually broadened, and the two upper levels of 5d states of Eu^{2+} ions could be no more observed.

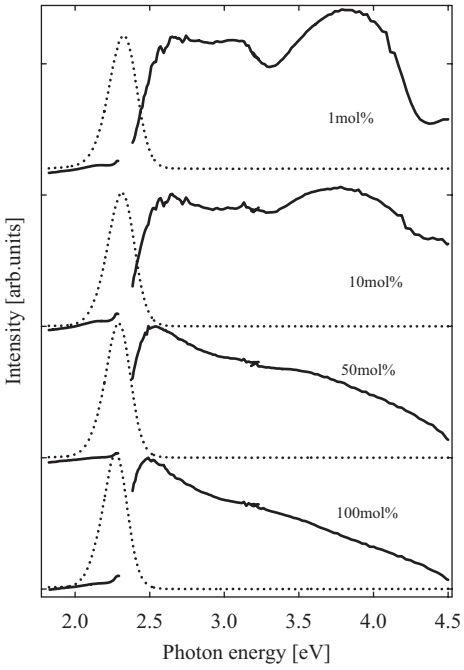

Fig. 4. The excitation spectra of $Sr_{1-x}Eu_xGa_2S_4$ with 1, 10, 50 and 100 mol%. The spectra are normalized by the intensity at 2.5 eV. A peak at 3.8 eV decreases with increasing Eu concentration.

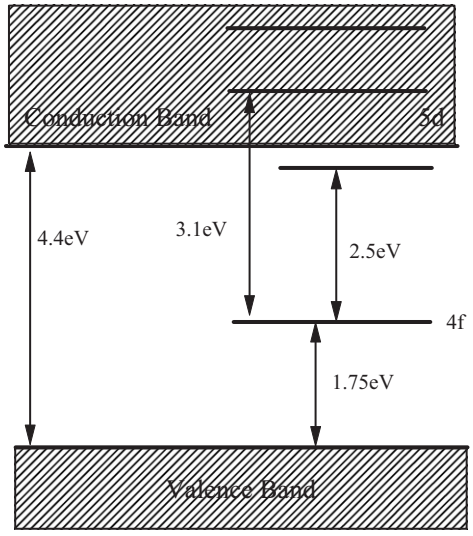

Fig. 5. Energy levels of Eu^{2+} in $Sr_{1-x}Eu_xGa_2S_4$. The 4f level locates at 1.75 eV from valence band. The upper level of 5d states sites in conduction band.

6. Summary

We have confirmed the solid solution in the $SrGa_2S_4$–$EuGa_2S_4$ system. It is shown that the Sr atoms can be continuously replaced by the Eu atoms. The integrated PL intensity has maximum at 10 mol% ($x = 0.1$). The PL intensity of the optimum compound is 3.5 times stronger than that of $EuGa_2S_4$. The quantum efficiency will approximately reach 75%. The PL peak energy shifts to the lower energy side due to the stronger crystal field when Eu concentration increases. We have determined the energy level of Eu^{2+} in the band diagram of $Sr_{1-x}Eu_xGa_2S_4$.

The compound with 10 mol% Eu^{2+} is suitable for the laser material and its crystal growth is now under way.

Acknowledgments

This work is partly supported by the grant for the high-technology research center project for private universities from the Ministry of Education, Sports, Science, Culture and Technology, Japan.

References

[1] T.E. Peter, J.A. Baglio, J. Electrochem. Soc. 119 (1972) 230.
[2] W.A. Barrow, R.C. Coovert, E. Dickey, C.N. King, C. Laakso, S.S. Sun, R.T. Tuenge, R. Wetross, J. Kane, in: SID International Symposium Dig., 1993.
[3] Y. Inoue, K. Tanaka, S. Okamato, K. Kobayashi, I. Fujimoto, Jpn. J. Appl. Phys. 34 (1995) 180.
[4] I.R. Limousin, A. Garcia, C. Fouassier, C. Barthou, P. Benalloul, J. Benoit, J. Electrochem. Soc. 144 (1997) 687.
[5] Y. Nakanishi, N. Uekura, F. Nakano, Y. Hatanaka, J. Lumin. 72 (1997) 373.
[6] T. Yang, B.K. Wangner, M. Chaichimansour, W. Park, Z.L. Wang, C.J. Summers, J. Vac. Sci. Technol. (1996) 2263.
[7] M.C. Nostrand, R.H. Page, S.A. Payne, W.F. Krupke, P.G. Schunemann, Opt. Lett. 24 (1999) 1215.
[8] S. Iida, T. Matsumoto, N.T. Maruyama, A.I. Bayramov, B.G. Tagiev, O.B. Tagiev, R.B. Dzhabbarov, Jpn. J. Appl. Phys. 36 (1997) 857.
[9] H. Najafov, A. Kato, H. Toyota, K. Iwai, A. Bayramov, S. Iida, Jpn. J. Appl. Phys. 41 (2002) 1424.
[10] S. Iida, A. Kaoto, M. Tanaka, H. Najafov, H. Ikuno, J. Phys. Chem. Solids 64 (2003) 1815–1819.
[11] C. Hidaka, E. Yamagishi, T. Takizawa, J. Phys. Chem. Solids 66 (2005) 2058–2060.
[12] R.D. Shannon, Acta Crystallogr. A32 (1976) 751.
[13] C. Chartier, C. Barthou, P. Benalloul, J.M. Frigerio, J. Lumin. 111 (2005) 147–158.
[14] P. Dorenbos, J. Crystal Growth 237–239 (2002) 2009–2013.
[15] P. Dorenbos, J. Lumin. 104 (2003) 239–260.

Available online at www.sciencedirect.com
ScienceDirect
Journal of Physics and Chemistry of Solids 69 (2008) 400–403
JOURNAL OF PHYSICS AND CHEMISTRY OF SOLIDS
www.elsevier.com/locate/jpcs

Crystal growth study of $CaGa_2S_4$ Co-doped with Ce^{3+} and Na^+

Shinya Oikawa, Chiharu Hidaka, Takeo Takizawa*

Department of Physics, College of Humanities and Sciences, Nihon University 3-25-40 Sakurajousui, Setagaya-ku, Tokyo 156-8550, Japan

Abstract

We have examined the effects of co-doping of Ce^{3+} and Na^+ in $CaGa_2S_4$. Differential thermal analysis and X-ray diffraction analysis were carried out on the compounds of $Ca_{(1-x)}Ce_{x/2}Na_{x/2}Ga_2S_4$ ($0 \leqslant x \leqslant 1$) to obtain the necessary information for their synthesis. It is shown that Ce^{3+} and Na^+ can be simultaneously doped into $CaGa_2S_4$ up to about 30 mol% ($x = 0.6$). The melting point was determined as a function of x. Photoluminescence (PL) was measured with these products, where the maximum intensity was found at 10 mol% ($x = 0.2$). Single crystals of $Ca_{(1-x)}Ce_{x/2}Na_{x/2}Ga_2S_4$ ($x = 0.02$ and 0.2) were grown from melt by the horizontal Bridgman method. Light absorption was measured near the fundamental absorption edge using a high quality part of the single crystals. Photoluminescence excitation (PLE) spectra were also measured using compounds of $Ca_{(1-x)}Ce_{x/2}Na_{x/2}Ga_2S_4$ with $x = 0.02$, 0.2 and 0.5 and a Ce only-doped $CaGa_2S_4$:Ce^+ (0.8 mol%).

Keywords: A. Inorganic compounds; D. Luminescence; D. Optical properties

1. Introduction

Alkaline earth thiogallates (MGa_2S_4, M = Ca, Sr, Ba) have wide band gaps appropriate for host materials of luminescent devices. Especially it is known that the compounds doped with rare-earth elements radiate light of various colors with high efficiency [1,2]. These compounds were first studied by Peters and Baglio [1]. An electroluminescence (EL) device made of $CaGa_2S_4$:Ce^{3+} compounds was first fabricated by Barrow et al. [3]. Since then, $CaGa_2S_4$ and $SrGa_2S_4$ have attracted much attention as host materials of EL devices, and many researches on photoluminescence (PL) and cathode luminescence (CL) have been carried out toward their application to full color displays.

On the other hand, a laser oscillation in a $CaGa_2S_4$:Eu^{2+} single crystal was reported by Iida et al. [4]. A laser action was also observed in a $CaGa_2S_4$:Dy^{3+} single crystal at 4.3–4.4 μm [5]. In view of the laser action, $CaGa_2S_4$ single crystals doped with Eu^{2+} or Ce^{3+} could be a good candidate for the wavelength tunable laser in the blue-green region because of the luminescence with a wide wavelength band. However, it is considered that the Ce^{3+} ion cannot be fully incorporated into $CaGa_2S_4$, since the charge balance is not established due to the difference in the valence of Ce and Ca ions. We have already reported that the single crystals grown from Ce^{3+} only-doped melt became blackish at Ce concentration of more than 0.8 mol% and became worse in crystal quality [6], which may arise from such charge imbalance.

In order to achieve a high concentration doping of Ce^{3+}, co-doping with alkaline ions such as Na^+ may be one of the best methods in view of the charge compensation with Ce^{3+} ions. It should also be noted that the average ion radius of Ce^{3+} and Na^+ (1.16 Å) in eight coordinations is almost as large as that of Ca^{2+} (1.14 Å) in the same atomic arrangement.

In what follows, the effects of co-doping of Ce^{3+} and Na^+ on the PL intensity are examined. Single crystal growth with a composition giving the maximum PL intensity has been tried.

2. Differential thermal analysis and X-ray diffraction of $Ca_{(1-x)}Ce_{x/2}Na_{x/2}Ga_2S_4$

Differential thermal analysis (DTA) measurement was carried out using mixtures of CaS, Ce_2S_3, Na_2S and Ga_2S_3.

*Corresponding author. Tel./fax: +81 3 5317 9772.
E-mail address: takiz@chs.nihon-u.ac.jp (T. Takizawa).

0022-3697/$ - see front matter © 2007 Elsevier Ltd. All rights reserved.
doi:10.1016/j.jpcs.2007.07.003

These compounds were weighed in Ar atmosphere to about 1 g in total in the stoichiometric composition. The weighed mixtures were put into quartz ampoules of 7 mmΦ (inner dia.) × 40 mm (length), the inner walls of which were coated by carbon, and sealed under the vacuum of 10^{-3} Torr. DTA measurements were run twice up to 1140 °C at a speed of 2 °C/min in both heating and cooling processes.

After DTA measurements, powder X-ray diffraction (XRD) patterns (Cu-Kα, 40 kV, 30 mA) were measured using the products prepared during the DTA measurements. As a result, it is found that the solid solution was formed between $CaGa_2S_4$ and $Ce_{1/2}Na_{1/2}Ga_2S_4$ in the concentration range from $x=0$ to about $x=0.6$ in $Ca_{(1-x)}Ce_{x/2}Na_{x/2}Ga_2S_4$. However, new diffraction lines which could not be assigned to any known compounds appeared above $x=0.6$.

The melting points of the compounds of $Ca_{(1-x)}Ce_{x/2}Na_{x/2}Ga_2S_4$ were determined by the second run of the DTA measurements. Fig. 1 shows the melting points in the concentration range from $x=0$ to $x=0.5$. The melting points of the compounds lowered as the concentration of Ce^{3+} and Na^+ increased.

The lattice constants and the unit cell's volume were shown to be almost independent of the Ce^{3+} and Na^+ concentrations. This may result from the fact that ion radius of Ca^{2+} (1.14 Å) is nearly equal to the average ion radius of Ce^{3+} and Na^+ (1.16 Å).

Though the phase diagram was not fully completed, we have tried to grow single crystals as described in Section 4.

3. PL of $Ca_{(1-x)}Ce_{x/2}Na_{x/2}Ga_2S_4$

To check the effect of co-doping on PL intensities, we measured PL spectra using the products after DTA under excitation of 325 nm light from a He–Cd laser (Omnichrome 3056-15M, 23 mW) together with a photonic multichannel analyzer (PMA11, HAMAMATSU) at room temperature. All the samples used were powdered and filled into quartz ampoules of 3 mmΦ (inner.dia) × 25 mm (length).

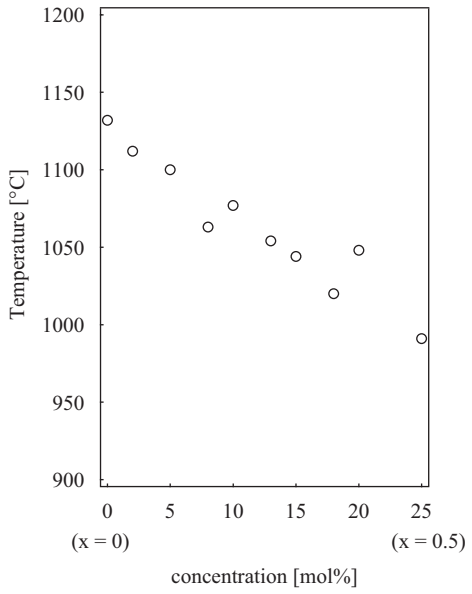

Fig. 1. Melting points of $CaGa_2S_4$-$Ca_{(1-x)}Ce_{x/2}Na_{x/2}Ga_2S_4$ ($x=0.5$) system obtained by DTA measurements.

Fig. 2 shows the PL spectra of $Ca_{(1-x)}Ce_{x/2}Na_{x/2}Ga_2S_4$ ($0 \leqslant x \leqslant 0.6$) and $CaGa_2S_4$:Ce (0.8 mol%). Two well-known emitting bands originating from the radiative transition between the 5d(T_{2g}) excited-state level and either 4f($^2F_{7/2}$) or 4f($^2F_{5/2}$) ground-state level of Ce^{3+} [1] found in the PL spectra. The integrated PL intensity as a function of composition x is shown in Fig. 3. It is interesting to note that the PL intensity of $Ca_{0.98}Ce_{0.01}Na_{0.01}Ga_2S_4$ is stronger than that of $CaGa_2S_4$:Ce^{3+} (0.8 mol%). The maximum PL intensity of $Ca_{(1-x)}Ce_{x/2}Na_{x/2}Ga_2S_4$ was attained at $x=0.2$ (10 mo%). Fig. 4 shows the peak energy shift of both bands as a function of the concentration of Ce^{3+} and Na^+ where the peaks energies of both bands shifted toward the lower energy side, indicating the strengthening of the crystal field with the doping concentration. This is explained by the lowering of the upper state d-band under the effect of the increase in the crystal field with the dopant concentration.

4. Crystal growth of $Ca_{0.98}Ce_{0.1}Na_{0.1}Ga_2S_4$

The compounds having two kinds of concentration of Ce^{3+} and Na^+ were tried for the crystal growth. One is 10 mol% ($x=0.2$) at which the PL shows the highest intensity and the other 1 mol% ($x=0.02$) for comparison to the former one and also to the 0.8 mol% (Ce only-doped) one already grown. CaS, Ce_2S_3, Na_2S and Ga_2S_3 were weighed to about 3 g in total in Ar atmosphere in order to prevent these compounds from oxidation. Weighed compounds were put in a quartz ampoule of

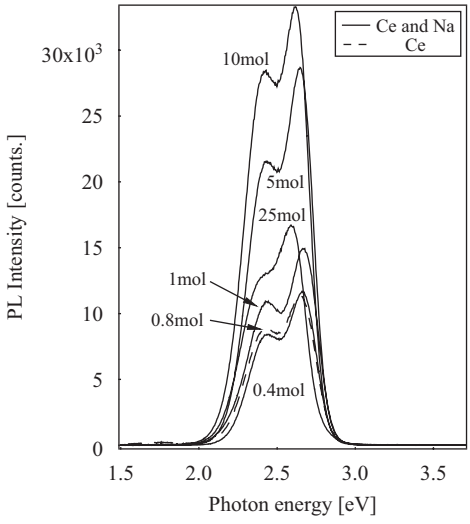

Fig. 2. Emission spectra of $CaGa_2S_4$:Ce (0.8 mol%) and $CaCaGa_2S_4$ doped with various Ce^{3+} and Na^+ concentration under excitation of 325 nm light from a He–Cd laser at room temperature.

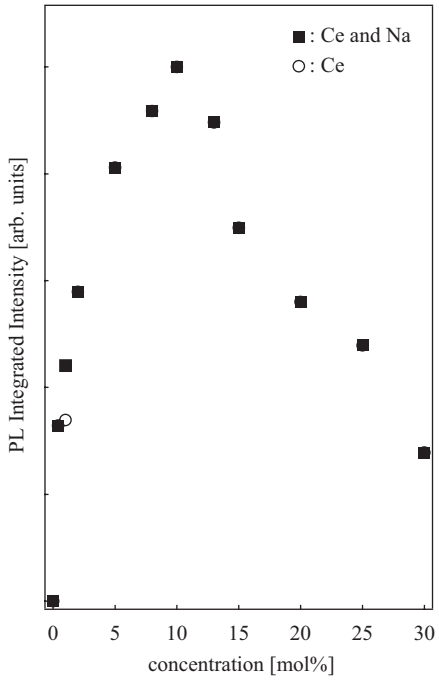

Fig. 3. Integrated emission intensity of $Ca_{1-x}Ce_{x/2}Na_{x/2}Ga_2S_4$ and $CaGa_2S_4$:Ce^{3+} 0.8 mol% as a function of x ($x = 0$–0.6). The concentration should be read as $(x/2) \times 100$.

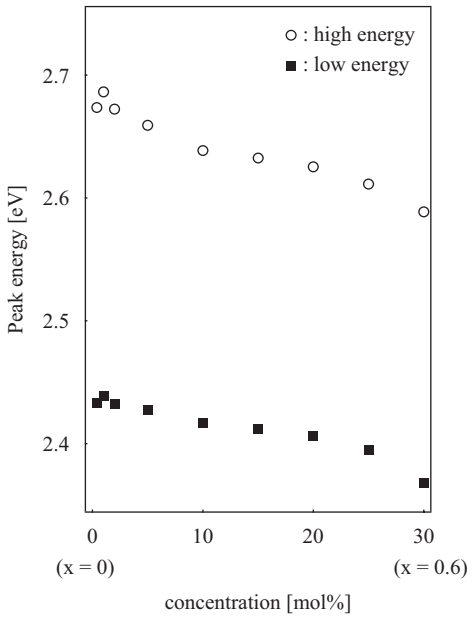

Fig. 4. Peak energy shift of PL spectra as a function of Ce^{3+} and Na^{+} concentration. The energy shifts to the low energy side with increasing Ce^{3+} and Na^{+} concentration. The A and B bands show the high and low energy parts of the Ce^{3+} emission.

7 mmΦ (inner dia.) × 100 mm (length) evacuated to about 1.0×10^{-6} Torr, inside of which was coated with carbon film as mentioned previously. The ampoule was set in another larger ampoule of 13 mmΦ (inner dia.) × 150 mm (length) and evacuated to about 1×10^{-6} Torr. The whole ampoule was elevated up to a temperature a little below the melting point. The precursors of 1 mol% ($x = 0.02$) and 10 mol% ($x = 0.2$) were prepared by the solid-state reaction; the synthesizing temperatures were determined based on the data of Fig. 1 as 1120 and 1070 °C, respectively. Each product after solid-state reaction was powdered and filled in another carbon boat of 8 mmΦ (inner dia.) × 100 mm (length) which was again sealed in a larger quartz ampoule. The ampoule was set in a furnace and a single crystal was grown from melt (one is kept at 1135 °C and the other at 1085 °C) by the horizontal Bridgman method. The speed of the growth was 0.25 cm/h.

A single crystal of the low dopant concentration was successfully grown, but no good crystal was obtained for the higher one ($x = 0.2$). This is because the compound with $x = 0.2$ exists just in the middle of the solid solution and its melting point sensitively changes with the dopant concentration. In addition, the Horizontal Bridgman method has a drawback that the composition of the grown crystal changes according to temperature variation. Thus for the success of the latter crystal growth, the strict control of both the melting temperature and the composition of the compound will be required.

5. Absorption and excitation spectra

Absorption spectrum was measured using a grown single crystal of $Ca_{0.98}Ce_{0.01}Na_{0.01}Ga_2S_4$. Light from a 300 W Xe lamp after passing through a monochromator (Bunkoh-Keiki, SM-25) was used for both absorption and excitation. Transmitted light was detected by a photomultiplier (HAMAMATU R562). Fig. 5 shows the absorption spectra of a $Ca_{0.98}Ce_{0.01}Na_{0.01}Ga_2S_4$ single crystal. The absorption peak due to Ce^{3+} was obtained at 2.9 eV. A shoulder which

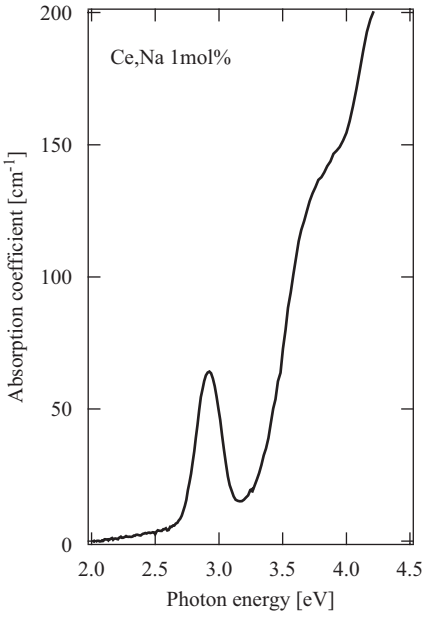

Fig. 5. Absorption spectrum of a $Ca_{0.98}Ce_{0.01}Ga_{0.01}Ga_2S_4$ single crystal. A peak and a shoulder appear at 2.9 and 3.6 eV, respectively.

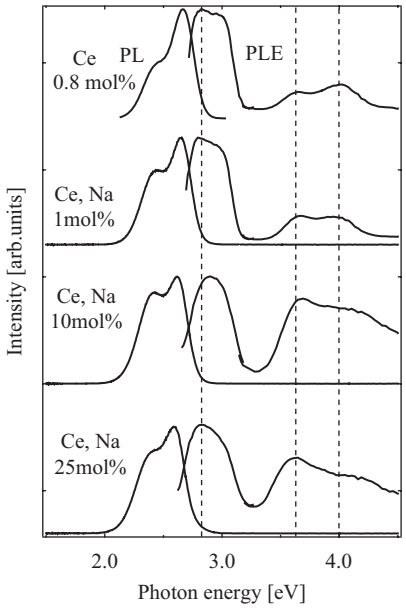

Fig. 6. PL and PLE spectra of a Ce^{3+} only-doped and Ce^{3+} and Na^{+} co-doped powdered compounds. PLE was monitored at the peak energy of PL (2.65 eV).

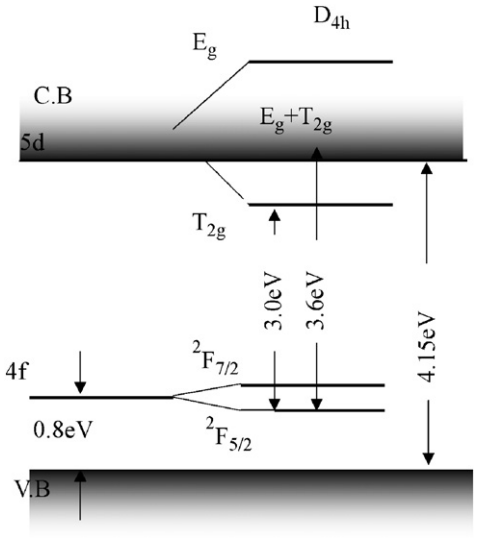

Fig. 7. Energy levels of Ce^{3+} in $CaGa_2S_4$ obtained from PL, PLE and absorption spectra.

was also due to the same ion was found at 3.6 eV just below the fundamental absorption edge of $CaGa_2S_4$.

For photoluminescence excitation (PLE) measurement, powdered samples of Ce 0.8, (Ce, Na) 1, 10 and 25 mol% were used. Measurements were carried out by monitoring at 2.65 eV of the PL spectrum using a monochromator (Nikon G250). Fig. 6 shows the PL and PLE spectra. It is known from this figure that the band widths and peak positions of PLE spectra did not depend on the concentrations of Ce^{3+} and Na^{+}. Several structures were found in PLE at 2.8, 3.0, 3.6 and 4.0 eV. The former three ones corresponded to the strong absorption bands due to the doped Ce^{3+} ions and the latter one (4.0 eV) to the fundamental absorption of the host compound. In reference to Fig. 6, we propose the energy diagram of Ce^{3+} in $CaGa_2S_4$ as shown in Fig. 7 [7].

6. Summary

The compounds of $Ca_{(1-x)}Ce_{x/2}Na_{x/2}Ga_2S_4$ $(0 \leqslant x \leqslant 1)$ were prepared to check the effect of co-doping of Ce^{3+} and Na^{+}. XRD patterns of these products showed that Ce^{3+} and Na^{+} could be doped into $CaGa_2S_4$ up to about 30 mol% ($x = 0.6$). The melting point was determined for each compound, and was shown to lower more than 100 °C as the concentration of Ce^{3+} and Na^{+} increased.

From PL measurements, the maximum intensity was found to be attained at 10 mol%. Two single crystals of $Ca_{0.98}Ce_{x0.01}Na_{0.01}Ga_2S_4$ and $Ca_{0.9}Ce_{0.1}Na_{0.1}Ga_2S_4$ were prepared by the horizontal Bridgman method, and the optical absorption was measured using a $Ca_{0.98}Ce_{x0.01}Na_{0.01}Ga_2S_4$ single crystal of better quality. PLE spectra of various concentrations of Ce^{3+} and Na^{+} were also measured. Based on these data, the electronic energy diagram of Ce^{3+} in $CaGa_2S_4$ was proposed.

Acknowledgments

This work was partly supported by Research Grant from Nihon University.

References

[1] T.E. Peters, J.A. Baglio, J. Electrochem. Soc. 119 (1972) 230–235.
[2] B.G. Tagiev, M.G. Shakhtakhtinskii, V.A. Dzhaliov, T.A. Gyul'maliev, B.M. Izzatov, G.K. Aslanov, O.B. Tagiev, Ya.G. Talybov, Inorg. Mater. 29 (10) (1993) 1238–1240.
[3] W.A. Barrow, R.C. Coóvert, E. Dickey, C.N. King, C. Laalso, S.S. Sun, R.T. Tuengo, R. Wentross, J. Kane, SID Int. Symp. Dig. (1993) 761.
[4] S. Iida, T. Matstumoto, N.T. Mamedov, A.N. Gyejong, Y. Maruyama, A.I. Bairamov, B.G. Tagiev, O.B. Tagiev, R.B. Dzhabbarov, Jpn. J. Appl. Phys. 36 (1997) L857.
[5] M.C. Nostrand, R.H. Page, S.A. Payne, W.F. Krupke, Opt. Lett. 24 (1999) 1215–1217.
[6] C. Hidaka, T. Takizawa, J. Cryst. Growth 237 (2002) 2009.
[7] A. Bessière, P. Dorenbos, C.W.E. van Eijk, E. Yamagishi, C. Hidaka, T. Takizawa, J. Electrochem. Soc. 151 (2004) H254–H260.

Available online at www.sciencedirect.com
ScienceDirect
Journal of Physics and Chemistry of Solids 69 (2008) 347–352
JOURNAL OF PHYSICS AND CHEMISTRY OF SOLIDS
www.elsevier.com/locate/jpcs

Single crystal growth of RE doped thiogallates and their optical properties

T. Takizawa*, C. Hidaka

Department of Physics, College of Humanities and Sciences, Nihon University, Sakura-Josui 3-25-40, Setagaya-ku, Tokyo 156-8550, Japan

Abstract

Rare earth (RE) elements of the lanthanide series are well known as light emitting sources when doped into transparent host materials. The mechanism of light emission due to these centers is rather well understood from both experimental and theoretical, but the detailed information concerning emitting efficiencies, spectral widths and quenching characteristics due to the RE ion concentration has not been fully obtained yet. To improve the emission efficiency and to control the functionality, now become the main issues to be addressed for their practical application to the light emitting devices. As the host materials for the RE centers above, alkaline earth thiogallates have long been expected as promising ones. However, most of the researches on these materials are carried out using polycrystalline thin films or polycrystals because of the difficulty in the single crystal growth arising from the high chemical reactivity along with high melting points of these compounds, so that the physical characteristics fundamental for the requirements mentioned above has not been fully clarified. Here, first we would like to introduce the details of our single-crystal growth method applied to Ca, Sr thiogallates, and then present the results of optical assessments for $CaGa_2S_4$ single crystals doped with several RE elements (Ce^{3+}, Pr^{3+}, Eu^{2+}, Tb^{3+}, Er^{3+}, Tm^{3+}). The optical transition levels of these ions are revisited in view of the calculated RE $4f^n$ energy level now easily available through the Internet (http://www.phys.canterbury.ac.nz/crystalfield/).

Keywords: A. Inorganic compounds; B. Chemical synthesis; D. Luminescence; D. Optical properties

1. Introduction

Rear-earth element (REE) doped compounds have attracted much attention because of their usefulness to the fluorescent applications. Actually, REEs are employed as luminescent centers in various materials for fluorescent tubes and also for LED light devices. Recently, the requirement for the illumination is strengthened and widen in accordance with the spread of our interest to various kinds of cultural fields. If much more proper materials are found, new devises and techniques for illumination as well as for light communication are expected to emerge to fulfill the broadened requirements of the illumination world.

From a viewpoint of the material science, we have to first search for proper materials and then pursue the research on their practical synthesis and crystal growth. Among the tremendous amount of candidates, we have confined our attention to the wide gap compounds belonging to the (Ca,Sr)–III_2–S_4 system [1,2]. These are simply contrived by changing the IIb element to the IIa one in the IIb–III_2–VI_4 system derivative of the adamantine compounds. Though the physical characteristics of the former are very different from those of the latter, especially in the electric properties, the wider band-gaps of the former thiogallates well suit for fluorescent host crystals.

The REE electronic energy levels important for luminescence have been well studied theoretically and are now available even through the web sites [3]. Actually, the energy level scheme of REE $4f^n$ electron configuration in several crystal lattices has been investigated, and an example is summarized as shown in Fig. 1 which is an energy band diagram of doubly and triply ionized REE ions in the $CaGa_2S_4$ lattice [4]. This figure shows that this compound may be a good candidate for luminescent devices, since many excited levels of 4f electrons are just within the band-gap. Another merit of these compounds is the surrounding of the doped REE ions. The crystal lattice

*Corresponding author. Tel.: +81 3 5317 9772; fax: +81 3 5317 9772.
E-mail address: takiz@chs.nihon-u.ac.jp (T. Takizawa).

0022-3697/$ - see front matter © 2007 Elsevier Ltd. All rights reserved.
doi:10.1016/j.jpcs.2007.07.017

forms in a complicated D_{2h}^{24}–Fddd structure consisting of 32 formula units in a unit cell, and the doped ion occupies the center of a decahedron having eight sulfur ions at each corner. Thus, the doped REE ion is rather isolated with other like ions, leading to the stability of luminescence against both temperature and doping concentration [5].

In general, powdered compounds are enough for the use in a passive manner by painting them on luminescent panels or walls inside of bulbs. Thus, almost all of the fluorescent compounds is synthesized and used in a form of polycrystalline powder doped with luminescent centers such as Mn^{2+}, Ce^{3+}, Eu^{2+} and Tb^{3+}. Regarding the single crystals of fluorescent compounds, much attention has not been paid so far. However, single crystals are inevitably needed for the physical characterization of the compounds. In addition, a new possibility to use them as an active device, e.g., wavelength variable laser devices, also emerges [6]. A laser action was already observed in $CaGa_2S_4:Eu^{2+}$ [6], though an emission induced decay was detected in a different species of the same compound [7].

Here, we present our method of synthesis of Ca and Sr thiogallates and their crystal growth. Optical properties of the compounds doped with various kinds of REE are also discussed.

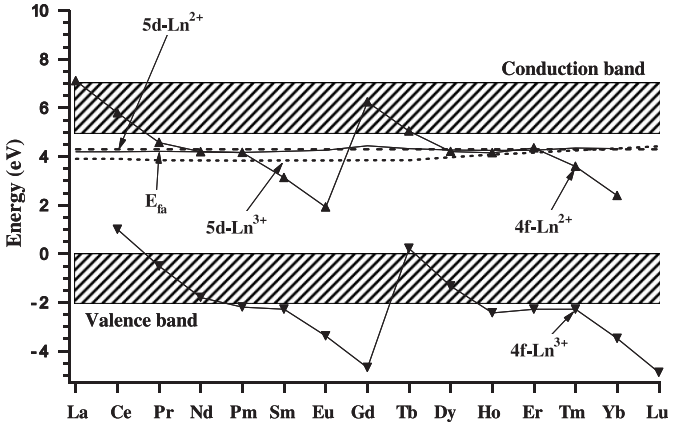

Fig. 1. Energy level scheme of divalent (▲) and trivalent (▼) lanthanides in $CaGa_2S_4$. The lowest 5d levels are also shown by the dotted (3+) and broken (2+) lines. The thin solid line indicates the fundamental optical absorption edge.

2. Single crystal growth

Ca, Sr and Ba thiogallates are well known as fluorescent materials with high efficiency of light emission when doped with Ce and Eu [1]. However, their synthesis was not so easy because of their high melting points and chemical reactivity. As a characteristic feature of sulfides, a sealed quartz ampoule of the products sometimes explodes at a high temperature. To escape from the explosion, we adopted the sulfurization technique when reacting starting materials such as CaS, SrS, Ga_2S_3 with each other. The purity of the starting materials was 99.9% for Ca and Sr shots, and 6% for Ga pellets and S powder. Ca or Sr sulfides of the same purity were also used. These were weighed in Ar atmosphere to about 5 g in total according to the chemical formulae, and then put into a carbon crucible and sealed in a quartz ampoule under vacuum of $\sim 1.0 \times 10^{-4}$ Pa. If S powder must be added, the S part was always set apart from the remaining materials in the ampoule to ensure the sulfurization. The temperature of the S part was kept at less than 450 °C, while the other end near the melting point of Ga_2S_3, where the whole chemical reaction took places, that is, all S was absorbed in this process. An appropriate amount (0.1–1 mol%) of REE was added in the synthesized compounds. Single crystals were grown in the horizontal Bridgman method using temperature profiles designed according to the binary or pseudo-binary phase diagrams already published for the systems of $CaS–Ga_2S_3$ and $SrS–Ga_2S_3$ [8,9]. Photos of the grown

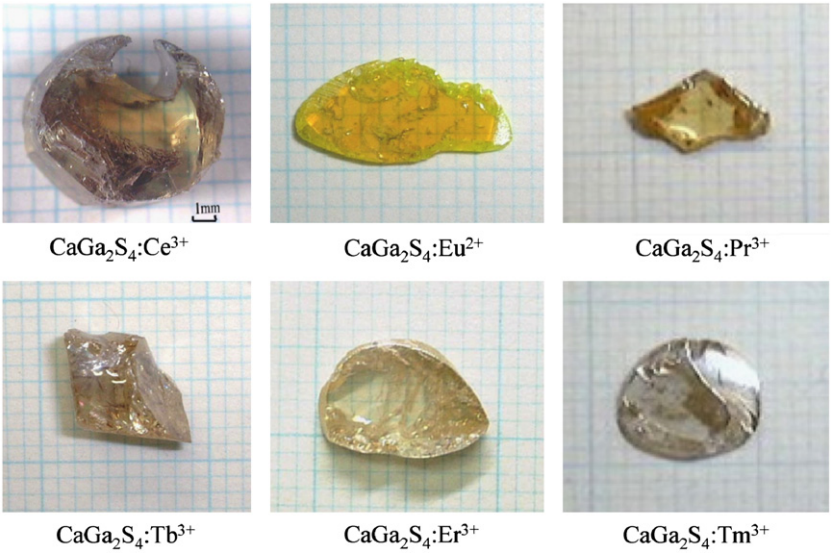

Fig. 2. REE doped single crystals of $CaGa_2S_4$. The concentration is 0.8 mol% for Ce and Eu and 0.5 mol% for Pr, Tb, Er and Tm.

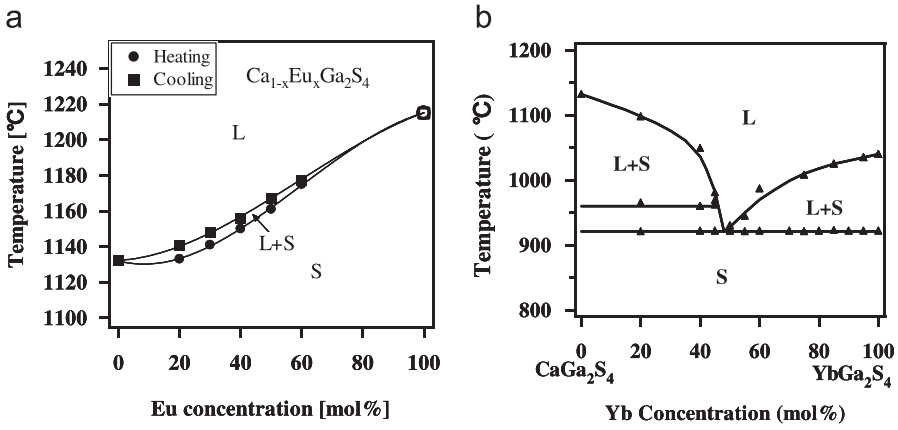

Fig. 3. The pseudo-binary phase diagrams: (a) $CaGa_2S_4$–$EuGa_2S_4$ and (b) $CaGa_2S_4$–$YbGa_2S_4$.

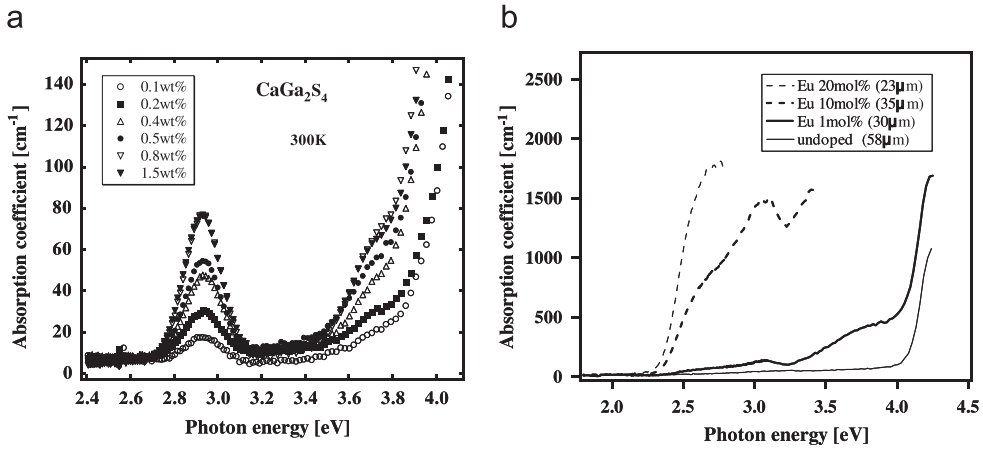

Fig. 4. Optical absorption of (a) doped Ce^{3+} ions (sample thickness of 60–120 μm) and (b) Eu^{2+} ions at different doping concentrations in $CaGa_2S_4$ single crystals.

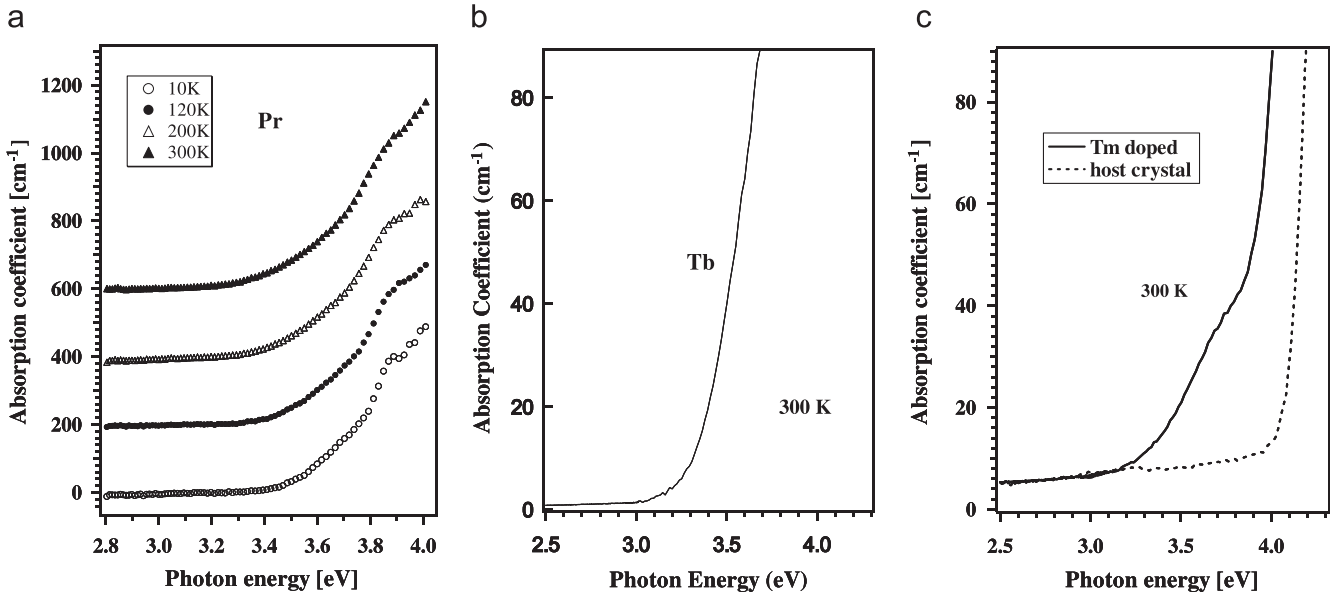

Fig. 5. Optical absorption of (a) Pr^{3+}, (b) Tb^{3+} and (c) Tm^{3+} ions in $CaGa_2S_4$ single crystals. The doping concentration is all 0.5 mol%. The temperature variation is small for these ions as shown in (a).

crystals doped with six kinds of REE are shown in Fig. 2, each of which was slightly colored but transparent and has cleaved surfaces.

Supercooling sometimes happened when a melt was cooled down to be solidified. In this case, a special care had to be taken to initiate the crystallization [10,11]. One method was to adopt a crucible with part of a small cross-section in one end and a larger one in a needed size in the other end [12].

3. Stoichiometric compounds and co-doping of REE

In the case of stoichiometric compounds such as $Ca_{1-x}Eu_xGa_2S_4$, Eu content can be freely varied. In Fig. 3(a), the phase diagram of the pseudo-binary system of $CaGa_2S_4$ and $EuGa_2S_4$ is shown, indicating a solid solution at any Eu content. We have confirmed that $Sr_xEu_{1-x}Ga_2S_4$ formed a similar solid solution. However, in the case of $Ca_xYb_{1-x}Ga_2S_4$, no solid solution was found but the

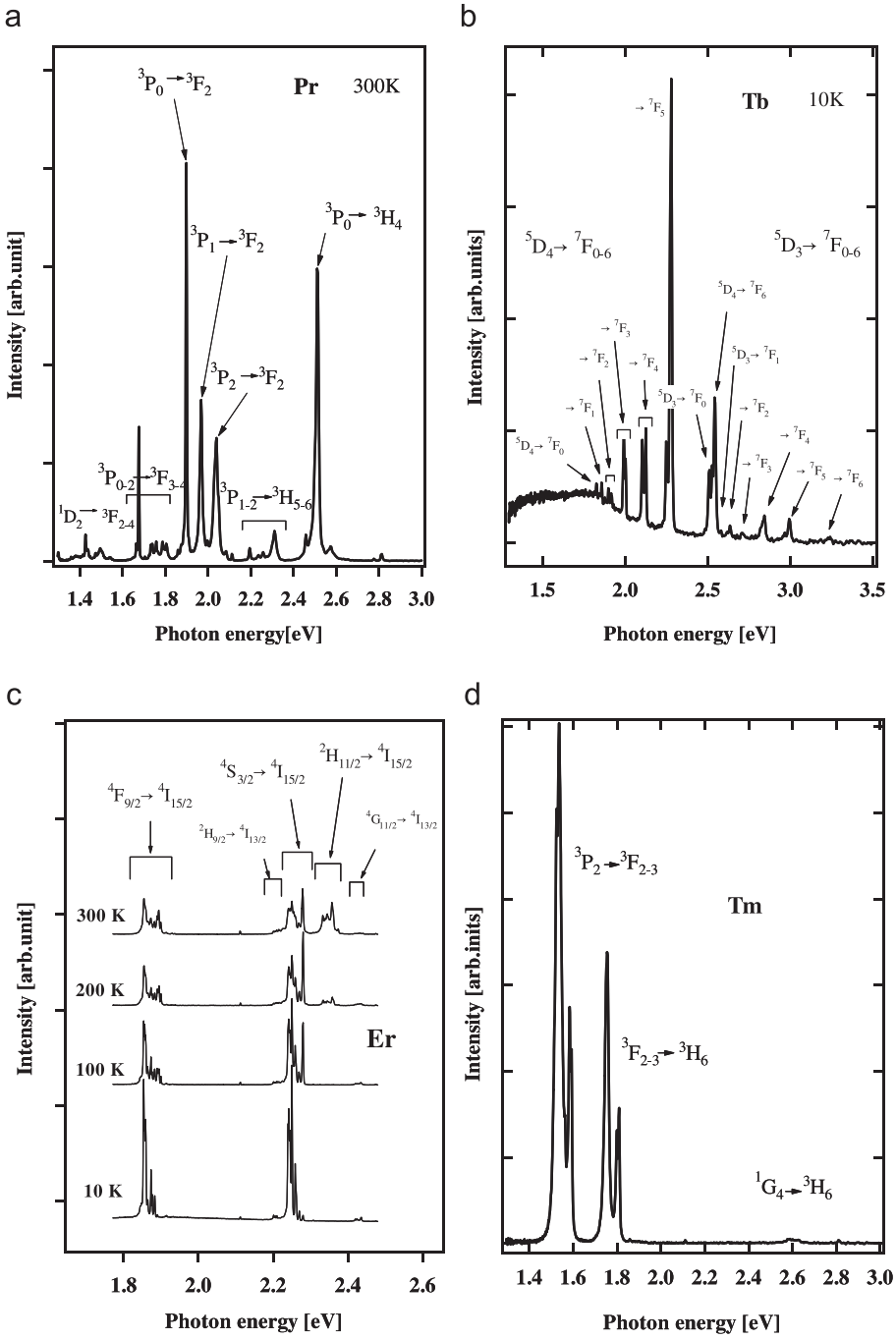

Fig. 6. Photoluminescence spectra of (a) Pr^{3+}, (b) Tb^{3+}, (c) Er^{3+} and (d) Tm^{3+}. The spectral assignments were performed in reference to the diagram of Carnall et al. [16].

eutectic reaction took places as shown in Fig. 3(b). Since the ion radii of Ca^{2+} and Yb^{2+} are very close to each other (1.12 and 1.14 Å in the eighth coordination, respectively) and Yb^{2+} is belonging to the same family of Eu^{2+}, this separative character is difficult to understand.

In the growth process of single crystals, REE doping could not sometimes exceed some amount. For example, Ce could not be added more than 1 mol% in the Ca or Sr thiogallate without degrading the quality of the crystal. If one increased the amount of Ce more than 1 mol%, the grown crystal became black and a lot of cracks were generated inside. In this case, the so-called co-doping with an alkaline element was effective [1,13]. We have tried the co-doping of Ca and Sr thiogallates with alkaline metals of Li, Na and K. In each case, it was confirmed by powder X-ray diffraction that up to 20 mol% Ce doping was successfully achieved [14].

4. Optical properties

The electronic energy levels of REE ions have been well studied since several decades ago [15]. Recently, the calculation of energy levels between f-electron configurations is available by the "SPECTRA", being supplied and open through the web site (http://www.phys.canterbury.ac.nz/crystalfield/) [16]. Such calculation is now extended to the UV–VUV range [17]. Calculation in terms of the cluster model (DV-Xα) is also open for public, enabling us to get the energy levels of REE ions embedded in model clusters [18,19].

Among the 14 lanthanide elements, Ce, Eu and Yb show broad phonon terminated 4f–5d transitions, and the others show emission spectra consisting of narrow 4f–4f lines. Especially, the broad emission of Ce and Eu is of high quantum efficiency, and the thiogallates doped with these elements are regarded as promising for electroluminescence as well as for wavelength variable lasers when used in a form of single crystal [6,7,20].

One of the merits of single crystal is to measure the optical absorption of doped REEs directly. The optical absorption of these two elements is shown in Fig. 4(a) and (b); for the detailed information of Ce^{3+}, see the literatures already reported [9,20]. The broad absorption of Eu^{2+} ions below ~4.2 eV ($CaGa_2S_4$'s band-gap) in Fig. 4(b) shows an interesting feature, indicating the band structure variation from Ca- to Eu-thiogallates. The optical absorptions of Pr^{3+}, Tb^{3+} and Tm^{3+} in $CaGa_2S_4$ are shown in Fig. 5(a)–(c) respectively. In comparison with the energy diagram in Fig. 1, the absorptions of Ce^{3+}, Eu^{2+} and Tb^{3+} were considered to be due to the optical transition from the ionized 4f ground states to the corresponding lowest 5d excited states. However, those of Pr^{3+} and Tm^{3+} were assigned to the so-called charge transfer from the valence band to the lowest 5d level for the former ion and to the ground state of 4f level of the latter Tm^{2+} ions. The absorption spectra of other ions have not been measured except for those of powder samples. This is because good single crystals for which the thickness can be made thinner than 0.05 mm have not been grown at present. The measurements of absorption spectra for the remaining lanthanides are now in progress.

The f–f optical transitions of REE in $CaGa_2S_4$ were already reported partly by Georgobiani et al. [21]. However, their data of Pr, Er and Tm differ from ours, so that we again show our data obtained by using single crystals in Fig. 6(a)–(d); for other ions a similar research is now under way. The energy level assignments were tentatively done in comparison of the REE $4f^n$ energies in LaF_3 given by Carnall et.al. together with the calculating results using "SPECTRA" [3,14]. The assignments are summarized and shown in Fig. 7. In our study, the PL spectra of Pr, Tb and Tm showed little temperature variation, but those of Er did a large temperature dependence as shown in Fig. 6(c). This may be caused by the variation of electron population due to temperature, but the detailed mechanism is not yet clarified.

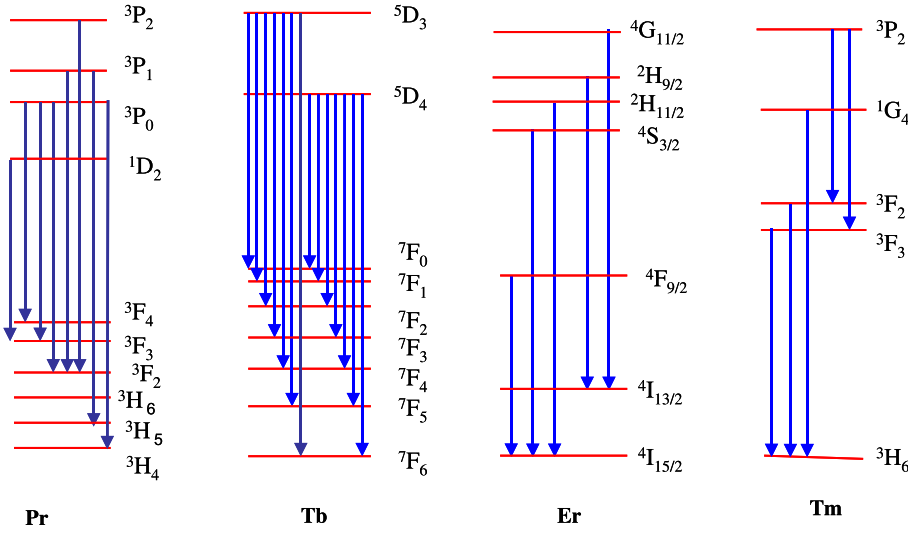

Fig. 7. Assigned energy levels for each ion.

5. Summary

The crystal growth method of REE doped Ca and Sr thiogallates were described. To escape from explosion sometimes occurring in the synthesizing process, the sulfurization method was adopted. In the case of super-cooling, a specially devised carbon crucible was shown to be effective. Triply ionized REE could be incorporated to an appropriate extent into a mother crystal by co-doping with alkaline metals, while doubly ionized ones except Yb formed the so-called stoichiometric compounds. It seems strange that Yb thiogallates could not mix with Ca ones.

The complex f–f transition energy levels can now be calculated using a program supplied by a theoretician group, enabling us relatively easily assigning the observed levels to the calculated ones. We feel that a time when we could freely design fluorescent materials according to our purpose is rapidly approaching.

Acknowledgments

We deeply thank Dr. A. Kato and Prof. S. Iida for the stimulating discussions and encouraging during the study. Thanks are also to Prof. P. Dorenbos for his collaboration and helpful discussions. This work is partly supported by the grant for the High-Technology Research Center Project for private universities from Ministry of Education, Sports, Culture and Technology, Japan.

References

[1] T.E. Peters, J.A. Baglio, J. Electrochem. Soc. 119 (1972) 230.
[2] P.C. Donohue, J.E. Hanlon, J. Electrochem. Soc. 121 (1974) 137.
[3] D.J. Newman, B. Ng (Eds.), Crystal Field Handbook, Cambridge University Press, Oxford, 2000.
[4] A. Bessière, P. Dorenbos, C.W.E. van Eijk, E. Yamagishi, C. Hidaka, T. Takizawa, J. Electrochem. Soc. 151 (2004) H254.
[5] K. Tanaka, Y. Inoue, S. Okamoto, K. Kobayashil, K. Takizawa, Jpn. J. Appl. Phys. 36 (1997) 3517.
[6] S. Iida, T. Matsumoto, N.T. Mamedov, G. An, Y. Maruyama, A.I. Bairamov, G. Tagiev, O.B. Tagiev, R.B. Dzhabbarov, Jpn. J. Appl. Phys. 36 (1997) L857.
[7] S. Iida, A. Kato, H. Najafov, C. Hidaka, T. Takizawa, in: Proceedings of International Conference ''Fizika-2005,'' Baku, Azerbaijan.
[8] C. Komatsu, T. Takizawa, J. Crystal Growth 210 (2000) 677.
[9] C. Hidaka, T. Takizawa, J. Crystal Growth 237–239 (2002) 2009; IPAP Book Series 1, Japanese Research Review for Pioneering Ternary and Multinary Compounds in the 21st Century, 2002, pp. 68–72.
[10] C. Hidaka, N. Makabe, T. Takizawa, J. Phys. Chem. Solids 64 (2003) 1797.
[11] C. Hidaka, M. Goto, M. Kubo, T. Takizawa, J. Crystal Growth 275 (2005) e439.
[12] T. Takizawa, M. Kubo, C. Hidaka, C. Hidaka, T. Takizawa, J. Crystal Growth 275 (2005) 433.
[13] J. Ronot-Limousin, A. Garcia, C. Fouassier, C. Barthou, P. Benalloul, J. Benoit, J. Electrochem. Soc. 144 (1997) 687.
[14] C. Hidaka, T. Takizawa, Papers presented at ISPN-2, Kaohsiung, 2005.
[15] K.W.H. Stevens, Proc. Phys. Soc. A65 (1951) 209.
[16] W.T. Carnall, G.L. Goodman, K. Rajnak, R.S. Rana, J. Chem. Phys. 90 (1989) 3443.
[17] J. Hölsa, M. Lastusaari, M. Maryško, M. Tuika, J. Solid State Chem. 178 (2005) 435.
[18] See the related web page.
[19] S. Nomura, T. Takizawa, S. Endo, in: Proceedings of 14th ICTMC, Denver, USA, 2004, J. Phys. Chem. Solid, in press.
[20] A. Kato, M. Yamazaki, H. Najafov, K. Iwai, A. Bayramov, C. Hidaka, T. Takizawa, S. Iida, J. Phys. Chem. Solids 64 (2003) 1511.
[21] A.N. Georgobiani, B.G. Tagiev, O.B. Tagiev, B.M. Izzatov, Inorg. Mater. 31 (1995) 16–19.

Available online at www.sciencedirect.com
SCIENCE DIRECT
Journal of Physics and Chemistry of Solids 66 (2005) 2090–2093
JOURNAL OF PHYSICS AND CHEMISTRY OF SOLIDS
www.elsevier.com/locate/jpcs

Electronic states of lanthanide in the ternary thiogallate $CaGa_2S_4$

Shigetaka Nomura [a,*], Takeo Takizawa [b], Saburo Endo [a]

[a] Department of Electrical Engineering, Faculty of Engineering, Tokyo University of Science, 1-3 Kagurazaka, Shinjuku-ku, Tokyo 162-8601, Japan
[b] Department of Physcis, College of Humanities & Sciences, Nihon University 3-25-40 Sakurajosui, Setagaya-ku, Tokyo 156-8550, Japan

Abstract

The electronic states of lanthanide (Ln) doped $CaGa_2S_4$ are investigated by the molecular orbital calculations for a spherical cluster of $LnCa_8Ga_{12}S_{24}$ using the FORTRAN program DVSCAT on the basis of the Discrete Variational method with Xα potentials (DV-Xα). In view of the SCF convergence, the Ln-doped lattice should contract to 85–90% of the mother crystal around the Ln atom for the lightweight lanthanides from Ce to Sm. On the other hand, the lattice contraction is very small for the heavyweight lanthanides, especially for Er, Tm and Yb in contrast to the generally known *lanthanide contraction* for Ln^{3+} ions. This is probably attributed to the effective charges of Ln atoms calculated here to be less than +1 for all lanthanides contrary to the chemically accepted value of +3. The energy level scheme of 4f and 5d related molecular orbitals is proposed for each Ln substituting Ca in $CaGa_2S_4$, showing that the optical processes relating to the 5d→4f transition must be complicated especially for the lightweight Ln-doped $CaGa_2S_4$.

Keywords: A. Chalcogenides; A. Optical materials; C. Ab initio calculations; D. Electronic structure

1. Introduction

The ternary thiogallate $CaGa_2S_4$ doped with lanthanide (Ln) has recently been noticed as promising for a wavelength-tunable light emitter in the visible region [1–3]. Now, detailed knowledge on the opt-electronic mechanism is necessary for the materials design and device engineering. In this work, the electronic states of Ln-doped $CaGa_2S_4$ are investigated by the molecular orbital (MO) calculations for a spherical cluster of $LnCa_8Ga_{12}S_{24}$ using the FORTRAN program DVSCAT based on the Discrete Variational method with Xα potentials (DV-Xα) [4].

2. Calculation

2.1. The DV-Xα method

The DV-Xα is one of the cluster methods based on the first principle and all-electron calculation, suitable for investigating local electronic states of the constituent atoms. The calculating system consists of the SCF (self-consistent field) calculation in reference to the respective electrons occupying the atomic orbitals for all the atoms in a cluster. The convergence in the SCF calculation corresponds to the minimum in the total energy of the electronic system. An effective calculation can be performed by the discrete variational method and the usage of the Xα potentials in solving the secular equations to determine the eigen states of the molecular orbitals. In this work, the non-spin and non-relativistic calculations were performed as the first step of the electronically complicated system of Ln-doped $CaGa_2S_4$.

2.2. Cluster model

Ternary thiogallate $CaGa_2S_4$ belongs to the space group of *Fddd:2*, including 224 atoms in an orthorhombic unit cell of $a=2.0122$, $b=2.0090$, and $c=1.2133$ nm [5]. In this work, a spherical cluster of $Ca_9Ga_{12}S_{24}$ was used as a mother body for the electronic state calculation. One of the Ca sites is set to the cluster center surrounded by eight S atoms with a distance of about 0.3 nm. The centric Ca atom is substituted by a Ln atom for the calculation of the Ln-doped electronic states. Actually, the distance from Ln to the surrounding S atoms, d(Ln–S), and naturally to all atoms in the cluster must have been adjusted in order to achieve the SCF convergence of the MO calculation. In other words, a lattice deformation around a doped Ln atom can be estimated from the electronic state calculation.

* Corresponding author. Tel.: +81 3 3260 4272; fax: +81 3 5261 4805.
E-mail address: nomura@rs.kagu.tus.ac.jp (S. Nomura).

0022-3697/$ - see front matter © 2006 Elsevier Ltd. All rights reserved.
doi:10.1016/j.jpcs.2005.10.120

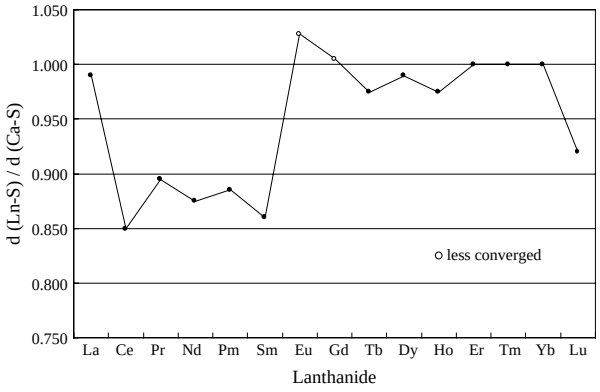

Fig. 1. Bond length d(Ln–S) variation normalized by that of the Ca–S bond, d(Ca–S), when the calculation converged.

3. Results and discussion

3.1. Lattice contraction by doping a Ln atom

Molecular orbital calculations were attempted on $LnCa_8Ga_{12}S_{24}$ clusters for full members of lanthanide. The SCF calculation converged only when all atomic positions in the cluster were rearranged from those in the mother cluster $Ca_9Ga_{12}S_{24}$ so as to properly adjust the specific distance between a Ln atom and surrounding eight S atoms. Fig. 1 shows the bond length d(Ln–S) variation normalized by that of the Ca–S bond, d(Ca–S) = 0.29672 nm, for full Ln members when the MO calculation converged. For the lightweight lanthanides from Ce to Sm, the lattice contracts to 85–90% of the mother cluster. The lattice contraction is very small for the heavyweight lanthanides, especially for Er, Tm and Yb. The best convergence was achieved for Yb without changing the lattice configuration around the cluster center of $Ca_9Ga_{12}S_{24}$. Both ends of the lanthanide series, La and Lu are exceptions whose 4f orbitals are completely empty and full, respectively. These results are different from the generally called *lanthanide contraction* for Ln^{3+} ions, where ionic radii become shorter with increasing the atomic number Z, or the number of 4f electrons. The difference comes from the fact that estimated effective charges for Ln atoms are less than +1, i.e. Ln^{+} instead of Ln^{3+}, as mentioned later.

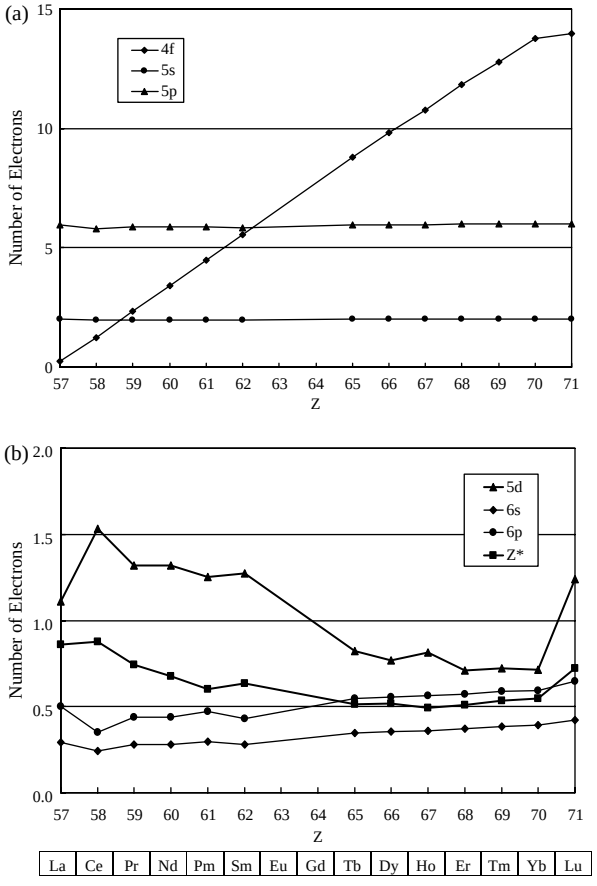

Fig. 2. The number of electrons in valence orbitals of (a) 4f, 5 s and 5p, and (b) 5d, 6 s, 6p and effective charge Z^* for the lanthanide series.

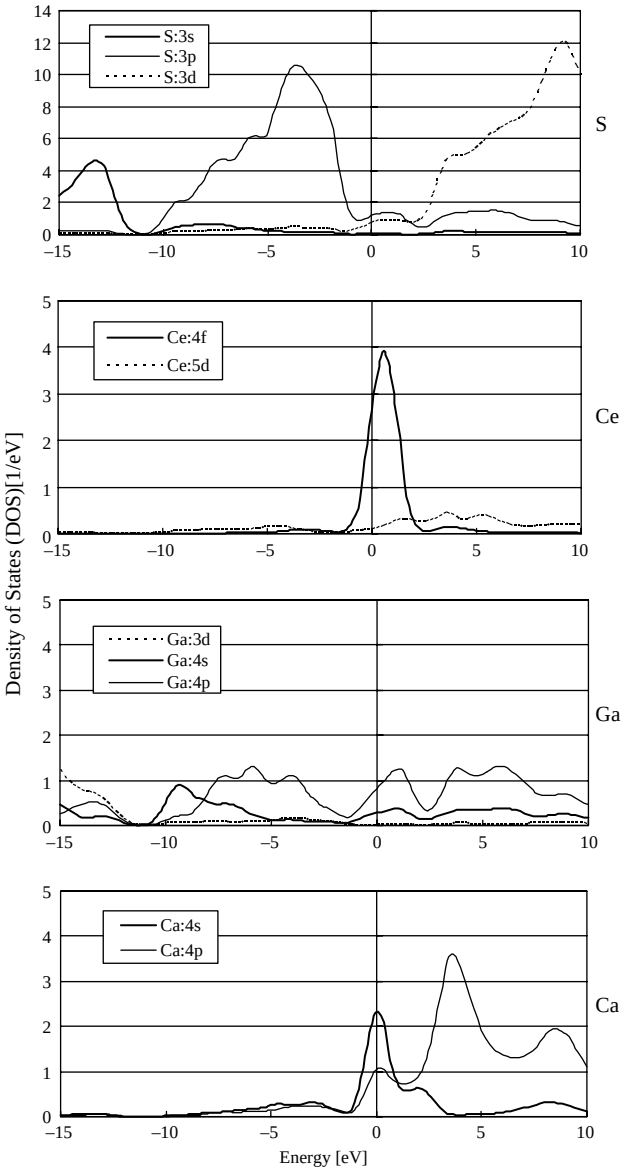

Fig. 3. Calculated density of states (DOS) of the atomic orbitals of the constituent elements for the Ce-doped $CaGa_2S_4$.

Table 1
Molecular orbitals relating to the 4f levels of Ce, showing the hybridization percentages for valence atomic orbitals of constituent elements

Energy (eV)	Ce				Ga			Ca		S		
	4f	5d	6s	6p	3d	4s	4p	4s	4p	3s	3p	3d
1.131	54	3	0	0	0	3	14	0	2	0	15	8
1.103	27	0	0	0	0	8	19	5	8	0	26	7
0.924	48	5	0	0	0	4	11	0	4	0	18	10
0.870	39	4	0	1	0	4	18	1	2	1	15	14
0.695	78	1	0	0	0	1	7	1	1	0	4	7
0.616	41	0	0	0	0	7	13	3	4	0	19	12
0.563	45	0	0	0	0	5	17	6	7	1	9	10
0.493	63	1	0	0	0	1	3	10	9	0	6	6
0.412	53	1	0	0	0	4	9	6	5	0	13	10
0.200	32	0	0	0	0	3	11	21	9	1	12	12
0.133	79	0	0	0	0	2	4	2	2	1	5	6
0.061	2	2	0	0	0	2	4	51	21	1	7	9
0.054	14	0	0	0	0	2	4	47	20	1	9	3
0.015	6	0	0	0	0	0	2	54	21	0	15	1
0	3	0	0	0	0	1	3	55	22	0	14	2
−0.100	1	2	0	0	0	4	13	40	14	1	13	12
−0.242	32	0	0	0	0	5	16	8	4	1	25	10

Sufficient convergence in the SCF calculation has not been achieved for Eu and Gd. For the two cases, we show the d(Ln–S)/d(Ca–S) ratios which minimize the respective mismatches in the SCF calculation. The ternary thiogallate $EuGa_2S_4$ has an orthorhombic unit cell of $a=2.0716$, $b=2.0404$ and $c=1.2200$ nm, belonging to the space group of *Fddd:2*, similar to $CaGa_2S_4$, [3]. From the crystal data, the bond length d(Eu–S) is estimated as 0.30094 nm which is slightly shorter than the d(Eu–S) = 0.30488 nm estimated from the SCF calculation.

3.2. Valence electrons of the lanthanide atoms

The valence electrons of each lanthanide atom were estimated from the MO calculations by the Mulliken's method, where covalent electrons are evenly shared with the bonding atoms. Fig. 2a shows the 4f, 5 s and 5p electrons for each lanthanide. The increment of the atomic number Z simply increments the number of the 4f electrons from La to Yb, while the 5 s and 5p orbitals are fully occupied for all lanthanides. Fig. 2b shows the 5d, 6 s, 6p electrons and effective charge Z^* as well. The number of the 5d electrons is calculated as the maximum of 1.53 for Ce, and gradually decreases to 0.71 for Yb with increasing Z, reflecting the decrease in the effective charge Z^* from 0.88 for Ce to 0.55 for Yb. This result poses a problem that the generally accepted feature of lanthanide ions in crystals as being trivalent or divalent is not necessarily true. The number of electrons occupying the outer 6 s and 6p orbitals slightly increases with increasing Z. The sum of them is no more than one for all lanthanides.

3.3. Molecular orbitals and the density of states of atomic orbitals

Fig. 3 shows the calculated density of states (DOS) of the respective atomic orbitals for the Ce-doped case, where the discrete DOS data are profiled with Gaussian type functions. The HOMO (highest occupied molecular orbital) level is set to be 0 eV here. Most of valence electrons belong to the 3p orbitals of S atoms. On the other hand, the hybrid orbitals of 3d of S, 4 s and 4p of both Ga and Ca form the unoccupied states. The 4f peak of Ce spreads around the HOMO level. Table 1 lists the molecular orbitals highly relating to the 4f orbitals of Ce, showing the hybridization percentage of the constituent atomic orbitals. Only one occupied level is seen for 4f orbital at −0.24 eV with the hybridization rate of 32%. Other MO levels relating to 4f are unoccupied states making strong hybridization mainly with the atomic orbitals of 4p of Ga and 3p and 3d of S. As can be seen in Fig. 3, the 5d atomic orbitals of Ce widely spreads in the unoccupied energy range, making many molecular orbitals strongly hybridizing with other unoccupied components such as 3d of S. On the other hand, there are some lanthanides showing weak hybridization on the 4f atomic orbitals such as Dy and Er.

3.4. Energy level scheme

Fig. 4 shows the energy level scheme of the molecular orbitals relating to 4f and 5d atomic orbitals of the Ln series except for Eu and Gd, because the SCF convergence was not

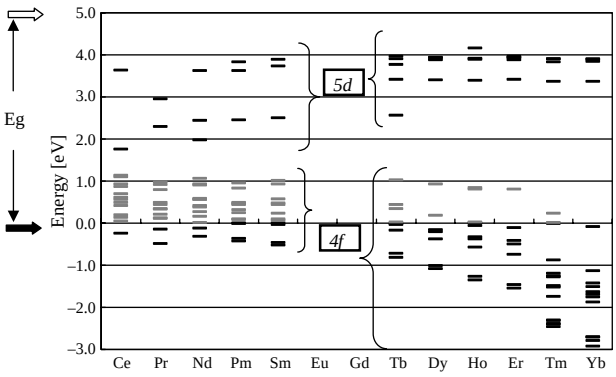

Fig. 4. Energy level scheme of 4f and 5d related molecular orbitals for the lanthanide series.

sufficient for the two cases. The highest occupied 4f level is directly below the HOMO level or corresponds to the HOMO level for all lanthanides. An increase in the number of the 4f electrons of Ln makes the relating molecular orbitals simply deeper in energy. On the other hand, the uppermost unoccupied 4f levels shown by the gray lines are located up to about 1 eV above the HOMO level. The unoccupied 5d related levels disperse in the midgap range for the lightweight Ln group, while those of the heavyweight group concentrate on the energy range of about 3.5–4 eV. The optical processes followed by the $5d \rightarrow 4f$ transition would be complicated because of the widely expanded 5d levels for the lightweight lanthanides, resulting in multiple and/or broad light emissions. In view of the expected density of states, the possibility or the efficiency is very small with respect to the visible light emissions brought by the $5d \rightarrow 4f$ transitions for the heavyweight lanthanides, from Dy- to Yb-doped cases.

4. Conclusion

The electronic states of lanthanide-doped $CaGa_2S_4$ were investigated from the molecular orbital calculations for spherical $LnCa_8Ga_{12}S_{24}$ clusters using the DV-Xα method. Substitution of Ln for Ca would induce some lattice contraction especially for the lightweight lanthanides from the view point of the SCF convergence in the molecular orbital calculation. Effective charges of the lanthanide elements when substituting Ca in $CaGa_2S_4$ are estimated to be less than $+1$ in contrast to the generally accepted trivalent assignments. An energy level scheme of the molecular orbitals highly relating to the 4f and 5d atomic orbitals for the lanthanide series in $CaGa_2S_4$ was proposed.

References

[1] S. Iida, T. Matsumoto, N.T. Mamedov, Y. Maruyama, A.I. Bairamov, B.G. Tagiev, O.B. Tagiev, R.B. Dzhabbarov, Jpn. J. Appl. Phys. 36 (1997) 857 Lett..
[2] A.N. Georgobiani, B.G. Tagiev, O.B. Tagiev, B.M. Izzatov, R.B. Jabbarov, Cryst. Res. Technol. 31 (1996) 849.
[3] T.E. Peter, J.A. Baglio, J. Electrochem. Soc. 119 (1972) 230–236.
[4] H. Adachi, M. Tsukada, C. Satoko, J. Phys. Soc. Jpn 45 (1978) 875.
[5] B. Eisenmann, M. Jakowski, W. Klee, H. Shäfer, Revue de Chimie minérale 20 (1983) 225.

Available online at www.sciencedirect.com
SCIENCE DIRECT
Journal of Physics and Chemistry of Solids 66 (2005) 2076–2078
JOURNAL OF PHYSICS AND CHEMISTRY OF SOLIDS
www.elsevier.com/locate/jpcs

Optical gain due to the Eu transition in the alloy of $Ca_{1-x}Eu_xGa_2S_4$

A. Kato [a,*], S. Iida [a,1], M. Yamazaki [b], E. Yamagishi [c], C. Hidaka [c], T. Takizawa [c]

[a] Nagaoka University of Technology, Kamitomioka 1603-1, Nagaoka 940-2188, Japan
[b] Nagaoka National College of Technology, Nagaoka 940-8532, Japan
[c] College of Humanities and Sciences, Nihon University, Tokyo 156-0045, Japan

Abstract

Room temperature photoluminescence quantum efficiency of the alloy of $Ca_{1-x}Eu_xGa_2S_4$ was measured as a function of x, and was found to be nearly unity under excitation at peak wavelength of excitation spectrum (510 nm) in the x range of $0.01 \leq x \leq 0.2$. At larger x values, it tends to decrease, but still as high as 30% for stoichiometric compound $EuGa_2S_4$. Taking these backgrounds into account, pump-probe experiments were done with $Ca_{1-x}Eu_xGa_2S_4$ for searching optical gain at $x=0.2$. The optical gain of nearly 30 cm^{-1} was confirmed to exist, though the pumping induced transient absorption which seems to limit the higher gain was found.

Keywords: A. Alloys; A. Optical materials; D. Luminescence; D. Optical properties

1. Introduction

Discussion [1] was given on laser application feasibility of the transition $^5D_1 \rightarrow {}^7F_2$ in Eu^{2+} [2] for the stoichiometric rare-earth compound of $EuGa_2S_4$, similarly to the case of $CaGa_2S_4$:Eu [3]. The alloy of these compounds $CaGa_2S_4$ and $EuGa_2S_4$, $Ca_{1-x}Eu_xGa_2S_4$, show an intense green–yellow Eu emission in the whole range of $0 \leq x \leq 1$ [4]. This alloy with proper x value, $Ca_{1-x}Eu_xGa_2S_4$, is expected to have an optical gain larger than $EuGa_2S_4$, since the Eu emission in the alloy with proper x is free from the concentration quenching. The present study concerns quantum efficiency measurements and an estimation of optical gain against x. The description also covers the result of pump-probe experiments for searching the gain at $x=0.2$.

2. Experimental

Single crystals of $Ca_{1-x}Eu_xGa_2S_4$ $(0.01 \leq x \leq 0.4)$ were grown by the Bridgeman method [4]. A single crystal of $EuGa_2S_4$ grown by iodine transport method was also used for quantum efficiency standard. In order to measure transient absorption under optical pumping, a crystal of $x=0.2$ was polished to be about 23 μm thickness.

Absolute PL quantum efficiency measurements were done using an integration semi-sphere as described in our reports [1,3] for two samples ($EuGa_2S_4$ and $Ca_{0.99}Eu_{0.01}Ga_2S_4$). For samples with other x values, relative intensities to these two samples with corrections taking into account the real absorption at corresponding x were treated as quantum efficiency values for these samples and plotted as x dependence of quantum efficiency.

The experimental setup of pump-probe experiments is shown in Fig. 1. An optical parametric oscillator (Spectra Physics, MOPO-SL) pumped by the third harmonic of a Q-switched Nd:YAG laser (Spectra Physics, PRO-230-10) was used as a pump source. Wavelength, pulse duration and maximum excitation density were 500 nm, 10 ns and 2 MW/cm^2, respectively. This wavelength nearly corresponds to the peak of the photoluminescence excitation band [1]. The 546 and 577 nm lines of a super high pressure Hg lamp (Ushio, USH-102B) were used as probe light. These wavelengths lie in the photoluminescence band.

The pumping light was monitored using a photo-diode by inserting a splitting plate in the pumping pass. Emission from the front side of the sample was dispersed through a monochromator (Ritsu, MC10) and detected by a photo-multiplier. Transmitted light of the probe light of the sample was dispersed by a monochromator (Jobin Ybon, HR-320) in conjunction with a photomultiplier (Toshiba, PM55). Pumping light, emission and transmitted light were recorded simultaneously by an oscilloscope (Sony Techtoronix, TDS 3054)

* Corresponding author. Tel.: +81 258 47 9542; fax: +81 258 47 9500.
E-mail address: arikato@vos.nagaokaut.ac.jp (A. Kato).
[1] Present address: Shizuoka Institute of Science and Technology, Fukuroi 437-8555, Japan.

0022-3697/$ - see front matter © 2005 Elsevier Ltd. All rights reserved.
doi:10.1016/j.jpcs.2005.09.057

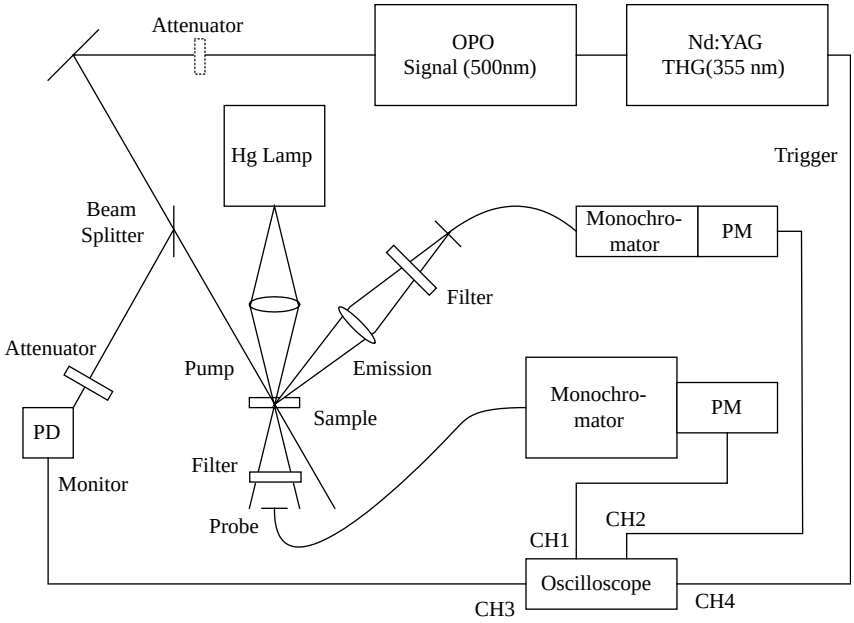

Fig. 1. Schematic diagram of arrangement of the pump-probe experiment.

with and without the probe light. All data were recoded using a single shot mode, since shot-to-shot fluctuation of the pump light was too large to be neglected.

The observed transmitted light included a spontaneous emission from the back side of the sample. Therefore, net intensity of transmitted light $I(t)$ was estimated by making a correction of this emission contribution with the following equation.

$$I(t) = I^{\mathrm{Tr}}_{\mathrm{Pu+Pr}}(t) - \frac{\int I^{\mathrm{Em}}_{\mathrm{Pu+Pr}}(t)\mathrm{d}t}{\int I^{\mathrm{Em}}_{\mathrm{Pu}}(t)\mathrm{d}t} I^{\mathrm{Tr}}_{\mathrm{Pu}}(t), \quad (1)$$

where $I^{\mathrm{Tr}}_{\mathrm{Pu+Pr}}(t)$ and $I^{\mathrm{Tr}}_{\mathrm{Pu}}(t)$ are temporal variations of the observed transmitted light with and without the probe light, respectively, and $I^{\mathrm{Em}}_{\mathrm{Pu+Pr}}(t)$ and $I^{\mathrm{Em}}_{\mathrm{Pu}}(t)$ are those of the observed emission with and without the probe light, respectively.

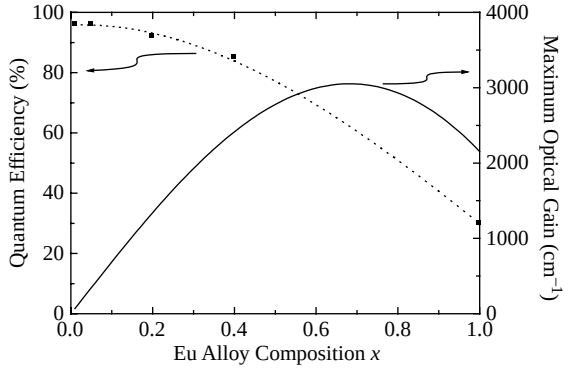

Fig. 2. Eu concentration dependence of the quantum efficiency under excitation at peak wavelength of the PLE spectrum at room temperature in $Ca_{1-x}Eu_xGa_2S_4$ system, and expected maximum optical gain according to the MacCumber's theory (see the text).

3. Results and discussion

Fig. 2 shows PL quantum efficiency vs. x relation. Actual measurements were done using the 441.6 nm laser line. The result shown in Fig. 2 is the efficiency vs. x relation corresponding the peak of the excitation spectrum at 510 nm [1]. Almost unit quantum efficiency of the luminescence is seen in the range $x \leq 0.2$ and the efficiency gradually decreased with x to $\sim 30\%$ for $x=1$ ($EuGa_2S_4$) at room temperature. Fig. 2 also shows x dependence of the maximum optical gain expected from the McCumber's theory [5] with the use of quantum efficiency corresponding to the dotted curve. The maximum optical gain as high as 3000 cm^{-1}, which is larger than that of $EuGa_2S_4$, is expected to be obtained at $x=0.7$ and the value of 1300 cm^{-1} is expected at $x=0.2$ where the pump-probe measurements were done.

Fig. 3(a) shows temporal variation of net intensity of the transmitted light $I(t)$. For comparison, temporal variation of the emission $I^{\mathrm{Em}}_{\mathrm{Pu}}(t)$ is shown in Fig. 3(b). The net intensity $I(t)$ shows an increase under the excitation, indicating the existence of optical gain. However, $I(t)$ turns to decrease to the level

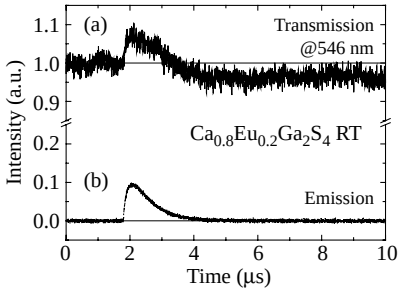

Fig. 3. Temporal variation of net intensity of the transmitted light $I(t)$ at 546 nm (a) correlated by Eq. (1) in the text and the emission (b) for pump-probe experiment of $Ca_{1-x}Eu_xGa_2S_4$ with $x=0.2$.

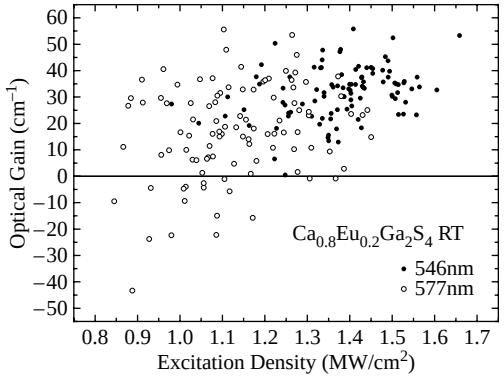

Fig. 4. Excitation density dependence of optical gain of $Ca_{1-x}Eu_xGa_2S_4$ with $x=0.2$. The value of optical gain was estimated from the increase of the transmitted light and the thickness of the sample. Closed and open circles show the optical gain measured by 546 and 577 nm probe light, respectively.

below the initial level, indicating the existence of the pumping induced transient absorption.

From the increase of $I(t)$ and the thickness of the sample, the optical gain value can be estimated. The results are shown in Fig. 4. Closed and open circles show the optical gain measured at 546 and 577 nm probe light, respectively. Most circles distribute in the range larger than 0, indicating the existence of optical gain. Closed circles for 546 nm probe light, which is close to the peak of the photoluminescence band, distribute around 30 cm^{-1}.

The number of photons per shot across unit area is

$$n_{\mathrm{ph}} = \frac{Pt}{\hbar\omega} = 2.5\times10^{16}\ \mathrm{cm}^{-2}, \tag{2}$$

where P is the excitation intensity (1 MW/cm^2), $\hbar\omega$ is the photon energy (2.5 eV (5000 Å)) and t is the pulse duration (10 ns) which is much smaller than the radiative lifetime of Eu ion (470 ns) [1]. The number of excited Eu ions per unit area is estimated to be

$$n_{\mathrm{Eu}} = \frac{d_{\mathrm{Eu}}}{\alpha} = 9.2\times10^{17}\ \mathrm{cm}^{-2}, \tag{3}$$

where d_{Eu} is the Eu density (1.2×10^{21} cm^{-3}) for Eu composition of $x=0.2$ and α is an absorption coefficient at wavelength of the pumping light which is assumed to be maximum optical gain $g_{\max}$ (1300 cm^{-1}) for Eu composition of $x=0.2$. The ratio of excited Eu ions to total Eu ions in the crystal is

$$\frac{n_{\mathrm{ph}}}{n_{\mathrm{Eu}}} = 0.027 \tag{4}$$

and optical gain is estimated to be

$$g = g_{\max}\frac{n_{\mathrm{ph}}}{n_{\mathrm{Eu}}} = 35\ \mathrm{cm}^{-1}. \tag{5}$$

Observed optical gain values in Fig. 4 distribute around 30 cm^{-1}, which corresponds to the optical gain estimated above. The gain in Fig. 4 does not show further increase with pumping intensity. This tendency is probably related to the emission saturation observed in Fig. 5. Even with the gain presently observed, laser construction is thought to be possible if a high quality crystal of 1 mm size can be obtained.

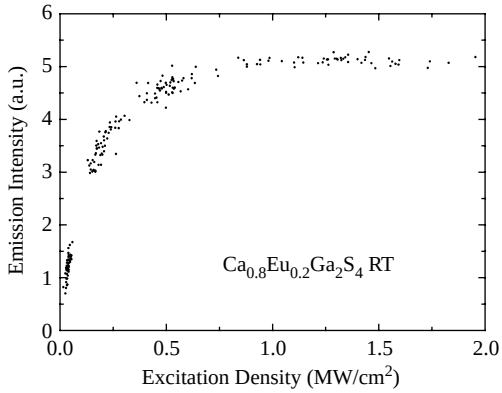

Fig. 5. Excitation density dependence of the emission intensity of $Ca_{1-x}Eu_xGa_2S_4$ with $x=0.2$.

Fig. 5 shows excitation intensity dependence of the emission intensity. The intensity of the emission shows saturation behavior at above 1 MW/cm^2. This saturation is probably related to the pumping induced transient absorption shown in Fig. 3(a). The origin of this saturation and the transient absorption is not clear at present. Re-absorption of trapped carriers can be considered as a candidate, since this alloy system shows thermoluminescence.

4. Summary

Room temperature photoluminescence quantum efficiency of the alloy of $Ca_{1-x}Eu_xGa_2S_4$ was measured as a function of x, and was found to be nearly unity under excitation at peak wavelength of excitation spectrum (510 nm) in the x range of $0.01\leq x\leq0.2$. At larger x values, it tends to decrease, but still as high as 30% for stoichiometric compound $EuGa_2S_4$.

Pump-probe experiments were done with $Ca_{1-x}Eu_xGa_2S_4$ for searching optical gain at $x=0.2$. The transmitted light showed an increase at initial stage, indicating an optical gain. However, it turned to decrease, indicating the existence of the pumping induced transient absorption. The value of observed gain at excitation density of 1 MW/cm^2 was nearly 30 cm^{-1}, which favorably compares with the theoretically estimated value based on the number of excited Eu ions corresponding to the excitation density. Even under this gain value, laser construction is thought to be possible if high quality crystals with 1 mm size are available.

The observed transient absorption seems to be related with observed intensity saturation of the emission under high excitation.

References

[1] S. Iida, A. Kato, M. Tanaka, H. Najafov, H. Ikuno, J. Phys. Chem. Solids 64 (2003) 1815.
[2] A.N. Georgobiani, B.G. Tagiev, O.B. Tagiev, B.M. Izzatov, R.B. Jabbarov, Cryst. Res. Technol. 31 (S-2) (1996) 849.
[3] S. Iida, in: T. Matsumoto et al. (Ed.), IPAP Books vol. 1, Institute of Pure and Applied Physics, Tokyo, Japan, 2001, p. 302.
[4] C. Hidaka, E. Yamagishi, T. Takizawa, to be presented in this Conference.
[5] D.E. McCumber, Phys. Rev. 134 (1964) A299.

Available online at www.sciencedirect.com
SCIENCE DIRECT
Journal of Physics and Chemistry of Solids 66 (2005) 2061–2064
JOURNAL OF PHYSICS AND CHEMISTRY OF SOLIDS
www.elsevier.com/locate/jpcs

Photoluminescence spectra of rare earth doped $CaGa_2S_4$ single crystals

C. Hidaka *, E. Yamagishi, T. Takizawa

Department of Physics, College of Humanities and Sciences, Nihon University, Sakura-josui 3-25-40, Setagaya-ku, Tokyo 156-8550, Japan

Abstract

Six kind $CaGa_2S_4$ single crystals doped with different rare earth (RE) elements are grown by the horizontal Bridgman method, and their photoluminescence (PL) spectra are measured in the temperature range from 10 to 300 K. The PL spectra of Ce or Eu doped crystals have broad line shapes due to the phonon assisted 4f–5d transitions. On the other hand, those of Pr^{3+}, Tb^{3+}, Er^{3+} or Tm^{3+} doped samples show narrow ones owing to the 4f–4f transitions. The assignments of the electronic levels are made in reference to the reported data of RE 4f multiplets observed in same materials.

Keywords: A. Optical materials; B. Crystal growth; D. Luminescence; D. Optical properties

1. Introduction

Rare earth (RE) elements of the lanthanide series are well known as light emitting sources when doped into transparent host materials. The mechanism of light emission in these materials is rather well understood from both experimental and theoretical [1–4], except for some detailed information such as emitting characteristics concerning efficiencies, spectral intensities and wavelengths. To improve the emission efficiency and to control the function are the central issues to be addressed for the materials mentioned above.

Alkaline earth thiogallates are long expected as promising hosts for visible light emitters. However, most of the researches on these materials are carried out using polycrystalline thin films or polycrystals, so that physical characteristics fundamental for the single crystal have not been fully clarified. Photoluminescence spectra of Ce and Eu doped crystals gave broad PL lines similar to those already described in previous papers [5,6]. Here, only the results of photoluminescence measured using $CaGa_2S_4$ single crystals doped with the respective elements (Pr^{3+}, Tb^{3+}, Er^{3+}, Tm^{3+}) successfully grown by the melt method are presented. These emission levels are discussed in comparison to those in the same hosts ever investigated [7].

2. Experimental procedures

The host compounds of $CaGa_2S_4$ were prepared using the elements of Ca, S and a compound of Ga_2S_3 weighed to 7 g in total in argon atmosphere. The detailed procedure is described elsewhere [8]. Rare earth elements were added at an amount of 0.5 wt% in a powder form of their sulfides. The crystal growth was performed in a horizontal Bridgman furnace at a growth speed of 2.5 mm/h. Four single crystals doped with different RE elements (Pr^{3+}, Tb^{3+}, Er^{3+}, Tm^{3+}) were grown. The EDX measurements show that each of them has a desired concentration of the doped RE element. The typical crystal size was approximately 6 mmϕ?×3 mm.

A He–Cd laser with 325 nm was used as a light source for excitation. For photoluminescence (PL) measurements, two kind spectrometers with a different resolution were used. Broad spectra were measured by a multi-channel detector (HAMAMATSU PMA-11) in the wavelength from 200 to 950 nm with resolution less than 2 nm, while narrow spectra by a spectrometer (Nikon G250) with resolution of 0.3 nm together with a photomultiplier (HAMAMATSU R562). A cut filter was placed in front of a detector for removing the scattered laser beam. Temperature variation of the spectra was observed between 10 and 300 K using a cryo-cooler.

Absorption spectra were measured with samples of 20 μm thickness using a deuterium or halogen lamp together with a monochromator (NALUMI RM-23) and a photomultiplier (HAMAMATSU R562) in the 10–300 K temperature range.

* Corresponding author. Fax: +81 3 5317 9772.
E-mail address: komaz@phys.chs.nihon-u.ac.jp (C. Hidaka).

0022-3697/$ - see front matter © 2005 Elsevier Ltd. All rights reserved.
doi:10.1016/j.jpcs.2005.09.068

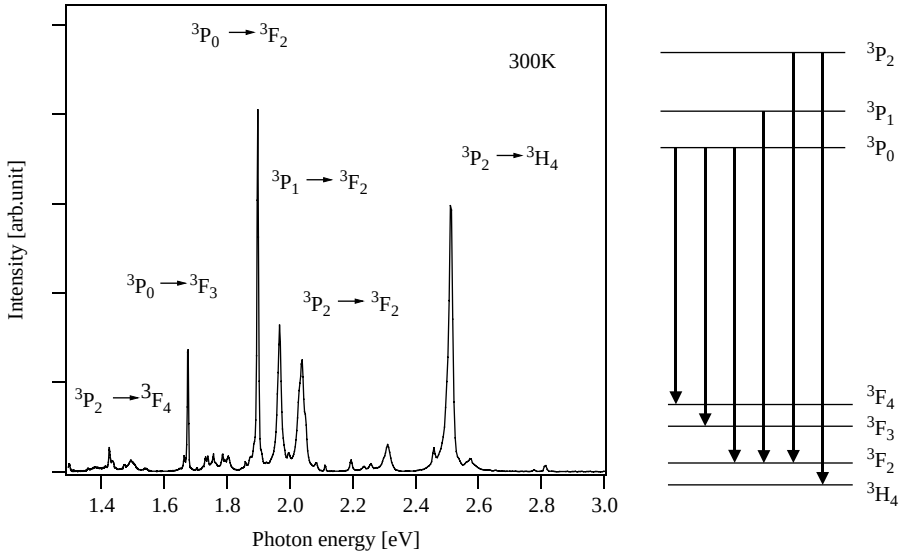

Fig. 1. Photoluminescence spectra of a Pr doped $CaGa_2S_4$ single crystal at 300 K. No difference of temperature variation was observed. A proposal assignment of the levels is shown in the right hand side.

3. Results and discussions

3.1. Photoluminescence

Fig. 1–4 show respective PL spectra of four $CaGa_2S_4$ single crystals each doped with one of the rare earth elements (Pr^{3+}, Tb^{3+}, Er^{3+}, Tm^{3+}), all consisting of sharp lines. Using samples prepared by solid state reaction and synthesis above 1200 °C, Georgobiani et al. already measured the PL spectra due to the RE elements above [7], which were however entirely different from the present ones. The main reason for this may be ascribed to the difference in sample preparations or to the difference in the excitation method (they used 365 nm line of mercury lamp as a light excitation source).

Fig. 1 shows the spectrum of a Pr doped crystal at 300 K. Its temperature variation was measured at 10, 100, 200 and 300 K, but no big difference was observed except a small broadening of the linewidth and a little enhancing of the line intensity with increase of temperature. The observed PL lines can be explained as the transitions between the 4f multiplets of Pr^{3+} ions [9]. A series of lines near 1.9 eV were identified as transitions between $^3P_0$, $^3P_1$, $^3P_2$ and $^3F_2$. Their energy differences were determined as 1.89, 1.97 and 2.03 eV, respectively. Two similar transition series corresponding to the transitions from ($^3P_0$, $^3P_1$, $^3P_2$) to $^3F_3$ and $^3F_4$ were observed

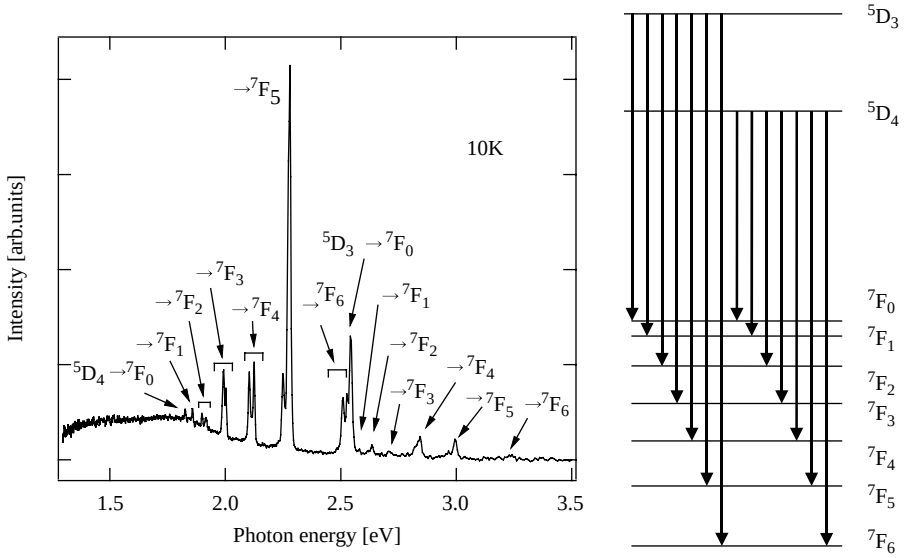

Fig. 2. Photoluminescence spectrum of a Tb doped $CaGa_2S_4$ single crystal at 10 K. Lines from 1.8 and 2.6 eV are almost not varied and those between 2.6 and 3.3 eV disappeared above 200 K. A proposal assignment of the levels is shown in the right hand side.

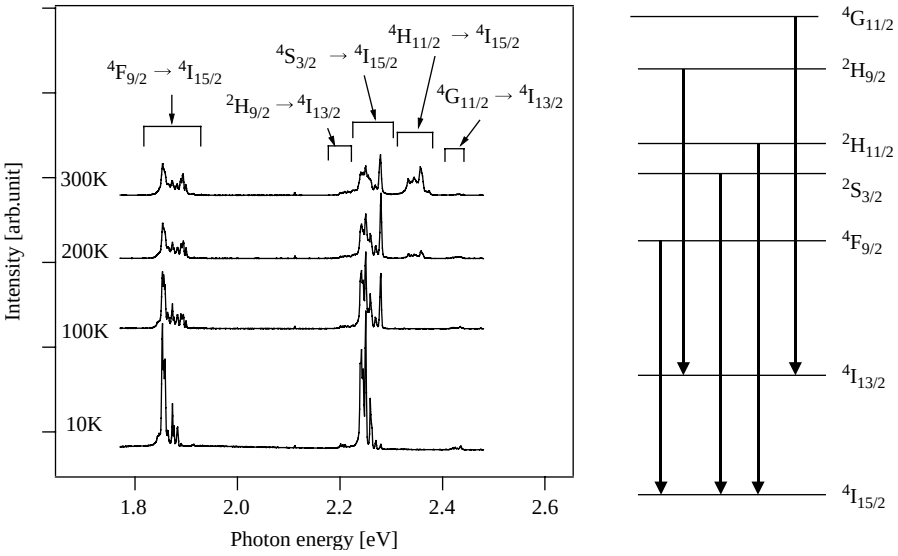

Fig. 3. Photoluminescence spectrum of an Er doped $CaGa_2S_4$ single crystal. Temperature variation from 10 to 300 K is also presented. There are two types of lines; appearing and diminishing with increasing temperature. A proposal assignment of levels is shown in the right hand side.

at 1.67 and 1.42 eV, respectively. The sharp structure at 2.50 eV was also interpreted as the lowest transition from $^3P_2$–$^3H_4$ in the transition group between ($^3P_0$, $^3P_1$, $^3P_2$) and $^3H_4$.

Fig. 2 shows the PL spectrum of a Tb doped crystal at 10 K. Sharp lines between 1.8 and 2.6 eV had almost no temperature variation, but those between 2.6 and 3.3 eV gradually lowered their intensity and disappeared above 200 K. The broad spectrum observed in the 1.3–2.0 eV range also disappeared above 200 K. Referencing the 4f electron configuration data [9], the fine structures between 1.8 and 2.6 eV were assigned to the transitions from $^5D_4$ to ^7F_i ($i=0$–6), the transition energies of which are 1.83, 1.86, 1.90–1.92, 1.99–2.00, 2.10–2.13, 2.25–2.28, 2.51–2.53 eV, where the hyphenation shows a doublet. The structures appearing in the 2.6–3.3 eV region were also assigned to the transitions from $^5D_3$ to ^7F_i ($i=0$–6), where each energy can be obtained by shifting each energy value mentioned above by 0.71 eV to the higher energy side. These spectra however diminished at higher temperature than 200 K. This may be attributed to the difference in characteristics between the excited states, that is, $^5D_4$ and $^5D_3$, since the electrons excited at the higher excited state $^5D_3$ may be more rapidly relaxed to the other lower states as temperature increases. A broad spectrum (1.3–2.0 eV) only observed at low temperatures was also observed in the X-ray excited PL spectra by Bessière et al. who proposed the self trapped exciton model for its interpretation [10]. To support their idea much experiment should be required.

The PL spectra of an Er doped crystal and their temperature variation were shown in Fig. 3. Yellow colored emission observed at low temperature changed its color to green as temperature increased. These spectra differ from those of the other RE doped thiogallates in a point that new lines appeared with increase of temperature (here after we say it as a 'positive' temperature dependence), in contrast that the lines at low temperature diminished or disappeared (we call it as a 'negative' one) in the other cases. Garcia et al. already measured Er doped thiogallates at 300 K [11]. Our data at the same temperature agreed very well with theirs, and the assignments according to them are shown in Fig. 3. On the base of these assignments, it can be inferred that among the PL ground states only the $^4I_{15/2}$ state may be the origin of the positive temperature dependence, since the lines assigned from $^4F_{9/2}$, $^4S_{3/2}$ and $^2H_{11/2}$ to $^4I_{15/2}$ showed positive ones, while those from $^2H_{9/2}$ and $^4G_{11/2}$ to $^4I_{13/2}$ showed the negative ones. The $^4I_{15/2}$ state is considered to spread out, i.e, it may consist of a band having some width. At low temperature, only the lowest energy part is occupied by electrons, so that the emission terminates at the higher energy part. As temperature increases, the empty states spread to the lower energy side in the $^4I_{15/2}$ band, and then the transition to the lower levels become allowed with temperature, which account for the appearing the new lines at the higher energy part at high temperatures in the transitions from $^4F_{9/2}$ and $^4S_{3/2}$ to $^4I_{15/2}$. On the other hand, the transition from $^2H_{11/2}$ to $^4I_{15/2}$ cannot be explained by this assumption.

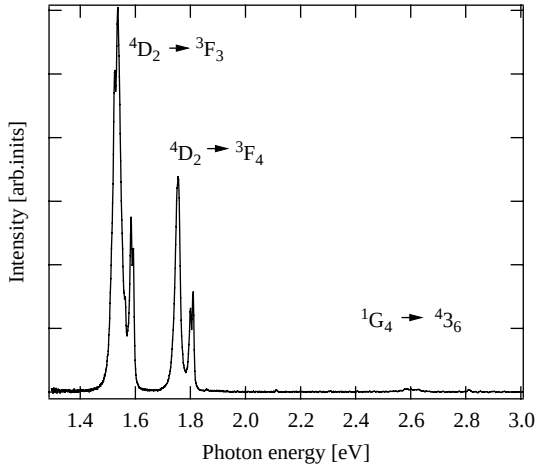

Fig. 4. Photoluminescence spectrum of a Tm doped $CaGa_2S_4$ single crystal at 300 K.

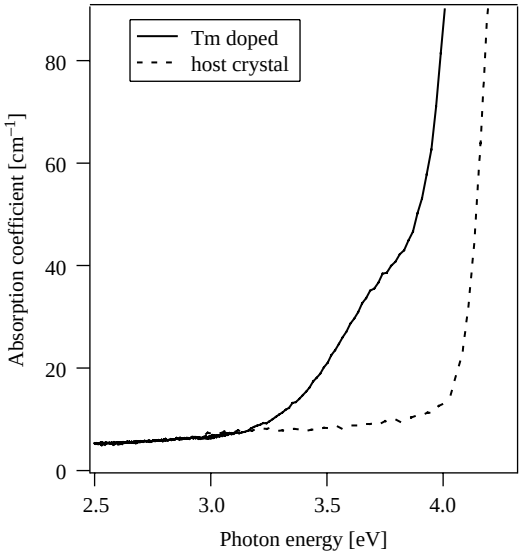

Fig. 5. Absorption spectra of Tm doped $CaGa_2S_4$ single crystal. The absorption spectra of a host crystal are also presented by the dashed line.

There may be some mechanisms that the $^2H_{11/2}$ state is populated only at high temperature. For the upper state of $^4I_{13/2}$, such phenomenon might not happen because of its narrow energy width, resulting in the normal temperature variation.

The photoluminescence spectrum of Tm doped crystal at 300 K was shown in Fig. 4, where temperature variation was not measured yet. A proposed assignment is shown in Fig. 4, but for the explanation of 1.5 eV lines (tentatively assigned as $^3H_4$–$^3H_6$), there still exist alternative ones, so that much experiment is required for the accurate assignment.

3.2. Absorption spectra

Optical absorption was measured for (Ce, Pr, Eu, Tb, Er, Tm) doped crystals. Their spectra were similar to each other, and therefore only a Tm case is shown in Fig. 5. Each RE ion gave an additional absorption band just below the fundamental optical band edge of the host crystal.

4. Conclusion

Six kind $CaGa_2S_4$ single crystals doped with different rare earth elements were grown by the horizontal Bridgman method, and their PL spectra were measured. These spectra were very different from those ever reported [7]. The PL spectra of Pr^{3+}, Tb^{3+}, Er^{3+} or Tm^{3+} doped ones presented sharp spectral shapes originating from the 4f–4f transitions, while those of Ce^{3+} or Eu^{2+} doped crystals were explained by the 4f–5d transitions in the RE electronic energy levels, resulting in broad line shapes owing to the phonon related transitions. The assignments of the electronic levels were performed in comparison to the reported data of RE 4f multiplets doped in same host materials.

Acknowledgements

This work is partly supported by the grant for the high-technology research center project for private universities from ministry of education, sports, science, culture and technology, Japan.

References

[1] T.E. Pters, J.A. Baglio, J. Electrochem. Soc. 119 (1972) 230–236.
[2] P. Dorenbos, J. Lumin. 104 (2003) 239–260.
[3] P. Dorenbos, J. Phys.: Condens. Matter 15 (2003) 575–594.
[4] E. Nakazawa, F. Shiga, Jpn. J. Appl. Phys. 42 (2003) 1642.
[5] A. Kato, K. Nadjafov, R. Hayashi, T. Matsumoto-Aoki, M. Yamazaki, B. Tagiev, R. Dzhabbarov, A. Bayamov, N. Mamedov, S. Iida, J. Appl. Phys. 39 (Suppl. 39-1) (2000) 440–441.
[6] C. Hidaka, E. Yamagishi, T. Takizawa, Preparation of Ca (1−x) EuxGa2S4 crystals and their photoluminescence, absorption and excitation spectra, J. Phys. Chem. Solids (2005).
[7] A.N. Georgobiani, B.G. Tagiev, O.B. Tagiev, B.M. Izzatov, R.B. Jabbarov, Cryst. Res. Technol. 31 (1996) 849–852.
[8] C. Hidaka, T. Takizawa, J. Cryst. Growth 237–239 (2002) 2009–2013.
[9] G.H. Dieke, Spectra and Energy Leveis of Rare Earth Ions in Crystals, Interscience, New York, 1968.
[10] A. Bessière, P. Dorenbos, C.W.E. van Eijk, E. Yamagishi, C. Hidaka, T. Takizawa, J. Electrochem. Soc. 151 (2004) H254–H260.
[11] A. Garcia, C. Fouassier, P. Doigier, J. Electrochem. Soc. 129 (1982) 2063–2069.

Available online at www.sciencedirect.com
SCIENCE DIRECT
Journal of Physics and Chemistry of Solids 66 (2005) 2058–2060
JOURNAL OF PHYSICS AND CHEMISTRY OF SOLIDS
www.elsevier.com/locate/jpcs

Preparation of $Ca_{(1-x)}Eu_xGa_2S_4$ crystals and their photoluminescence, absorption and excitation spectra

Chiharu Hidaka *, Eri Yamagishi, Takeo Takizawa

Department of Physics, College of Humanities and Sciences, Nihon University, 3-25-40 Sakurajosui, Setagaya-ku, Tokyo 156-8550, Japan

Abstract

The single crystal of $CaGa_2S_4$:Eu is expected as a useful laser material with a high quantum efficiency of light emission. However, as far as our knowledge is concerned, the systematic study of the mixed compounds of $Ca_{(1-x)}Eu_xGa_2S_4$ as a function of x has not been reported up to now. Here, we have first constructed the phase diagram of the $CaGa_2S_4$ and $EuGa_2S_4$ pseudo binary system, and show that it forms the solid solution. Then we have grown single crystals of these compounds. The maximum photoluminescence efficiency is achieved at $x=0.25$. From the three peak energies observed in the photoluminescence excitation (PLE) and absorption spectra, the 5d excited states are suggested to consist of three levels arising from the multiplets of Eu^{2+} ions.

Keywords: A. Optical materials; B. Crystal growth; D. Luminescence; D. Optical properties

1. Introduction

Rare earth element doped $CaGa_2S_4$ compounds are regarded as host materials for fluorescent devices [1]. Especially, Ce^{3+} or Eu^{2+} doped compounds exhibit strong emission caused by the 5d-4f electronic transitions [2,3]. In the case of Ce^{3+} doping, the photoluminescence (PL) intensity is limited below a certain value because the Ce^{3+} concentration could not be increased more than 1 mol% in the melt grown single crystals [4]. On the other hand, in the case of Eu doping, Ca atoms in $CaGa_2S_4$ can be substituted by Eu atoms in any amount and even 100% substitution by Eu is possible. Since the emission intensity is expected to increase with the Eu content, $EuGa_2S_4$ can be a profitable laser material with a high quantum efficiency of light emission [3,5]. However, too high concentration of Eu may cause the so-called concentration quenching to the photo-emission, so that an optimum Eu content may be expected in this material. In addition, it has been known difficult to prepare a $EuGa_2S_4$ single crystal by the melt growth using a quartz ampoule, because of the high melting point of 1215 °C [6]. On the other hand, that of $CaGa_2S_4$ is low enough to grow it in a sealed quartz ampoule. Thus we have tried to prepare $Ca_{(1-x)}Eu_xGa_2S_4$ compounds at various x values between 0 and 1 expecting to find an appropriate one for the laser action [7], and at the same time to find the upper limit value of x for the single crystal growth using quartz ampoules.

In this report, first we have constructed the phase diagram of the pseudo-binary system of $CaGa_2S_4$ and $EuGa_2S_4$ to obtain the necessary information on the crystal growth of the compounds above. Then using the powder compounds prepared in the process above, photo-luminescence (PL) and photo-luminescence excitation (PLE) are measured to investigate the relation between the efficiency of PL and the Eu concentration. Further, based on the phase diagram constructed, single crystals of $Ca_{(1-x)}Eu_xGa_2S_4$ compounds are grown for $x=0.01$, 0.02, 0.10 and 0.20. Optical absorption, PL and PLE spectra of these crystals are discussed together with the powder data.

2. Phase diagram and crystal growth

First, the pseudo-binary phase diagram for $Ca_{(1-x)}Eu_xGa_2S_4$ was constructed in the composition range from $x=0$ to 1 using differential thermal analysis (DTA) and powder X-ray diffraction (XRD). For DTA measurements, the elements of Ca and S as well as the compounds of EuS and Ga_2S_3 were weighed according to the designed prescription to approximately 0.3 g in total and sealed in a quartz ampoule of 7 mm$\phi\times$40 mm in vacuum. The inner wall of an ampoule was coated with carbon by firing acetone to avoid the fracture of an ampoule due to the chemical reaction between mixed elements and quartz. DTA measurements were carried out twice; the first

* Corresponding author. Fax: +81 3 5317 9772.

0022-3697/$ - see front matter © 2005 Elsevier Ltd. All rights reserved.
doi:10.1016/j.jpcs.2005.09.048

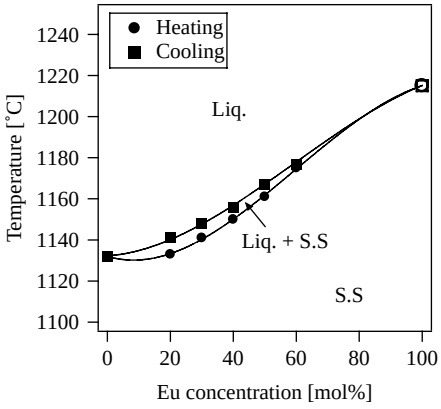

Fig. 1. Pseudo-binary phase diagram of the $CaGa_2S_4$–$EuGa_2S_4$. Solid solution (S.S) was found in the whole composition of Eu.

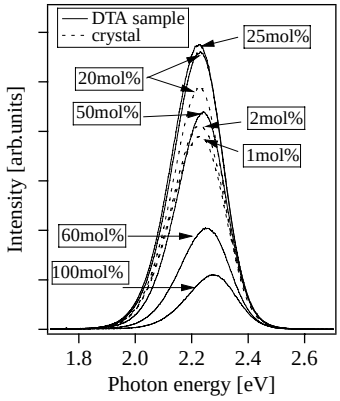

Fig. 2. Photoluminescence spectra of $Ca_{1-x}Eu_xGa_2S_4$ compounds. The maximum efficiency is observed at 25 Eu mol.%.

was to investigate the chemical reaction process and the second was to determine the phase transition points in the phase diagram. Using the products produced during DTA measurements, the lattice parameters of the compounds were determined by XRD, where a and b axes were shown to continuously increase and the c axis to decrease against the composition x. The resultant pseudo-binary phase diagram of the $CaGa_2S_4$–$EuGa_2S_4$ system is shown in Fig. 1. The solid solution was found in the whole composition range. Consequently, $Ca_{(1-x)}Eu_xGa_2S_4$ compounds are shown to be prepared at any value of x, i.e. the Ca ions can be continuously substituted by the Eu ions in the Ca thiogallate.

Single crystals of $Ca_{(1-x)}Eu_xGa_2S_4$ were grown at four x values of 0.01, 0.02, 0.10 and 0.20, using the same elements as used in DTA, weighed to approximately 5 g in total. A mixture of Ca, EuS and Ga_2S_3 was put on a quartz boat coated with carbon film. Here, the boat and the deficient amount of sulfur were separately set near the both ends of a long quartz ampoule (13 mm $\phi\times$280 mm). For sulfurizing the Ca element, the Ca part was set to 450 °C while keeping the S part at 300 °C for 24 h, where S was completely absorbed in the Ca part of the boat above, resulting in the CaS compound. Then the mixture was heated just above the melting point. After rapidly cooling it down, the resultant compound was taken out and ground. It was again put in a carbon crucible and sealed in a quartz ampoule in vacuum. The detailed growth procedure is described elsewhere [4].

As can be seen in Fig. 1, there observed a region, where the liquid and solid phases co-existed. Thus on naturally cooling down the composition deviation might be expected in a grown crystal. However, the region was rather narrow with respect to the composition x, so that the deviation might not be large. Actually, the composition of grown crystals was checked by an X-ray Guide Tube (EDX) to find that a desired-composition part ($x=0.21$–0.22) could be cut out from an ingot and was served for optical experiments.

3. Experimental procedure for optical measurements

PL measurements were carried out using a He–Cd laser (325 nm, 23 mW) as a light source for excitation together with the multi-channel detector (HAMAMATSU PMA-11) in the wavelength from 200 to 950 nm with resolution less than 2 nm. A cut filter was used for removing the scattered laser beam. Temperature variation was measured from 10 to 300 K. To eliminate the difference in size and shape of samples, polycrystals used for PL were powdered and filled into quartz capillaries with a same size of 3 mm $\phi\times$20 mm.

Excitation spectra were observed by a monochromator (Nikon G250) with a photomultiplier (MAMAMATSU R562) at 300 K at a PL peak of 2.2 eV using a 300 W Xenon lamp with a spectrometer (BUNKOKEIKI SM-25) as a light source. The grating in the latter spectrometer was blazed at 300 nm. The measurements were carried out using single crystals with compositions of $x=0.01$, 0.02, 0.10 and 0.20 having a size of 6 mm $\phi\times$3 mm.

Optical absorption was measured using a monochromator with a photomultiplier (HAMAMATSU R562) in the 10–300 K temperature range. The sample thickness was approximately 10 nm.

4. Photoluminescence, excitation and absorption spectra

Fig. 2 shows PL spectra of the compounds with various Eu mol.% at 300 K. The spectra were broad and similar to those previously observed [2]. Integrated PL intensities largely depended on Eu concentration and show a maximum near $x=0.25$ (see Fig. 3). The peak energy stays at a constant value

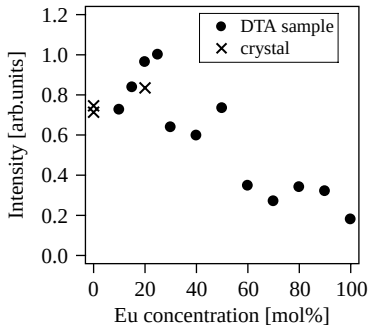

Fig. 3. Integrated intensity of photoluminescence at various concentrations of Eu. The intensity has the maximum at 25 Eu mol.%.

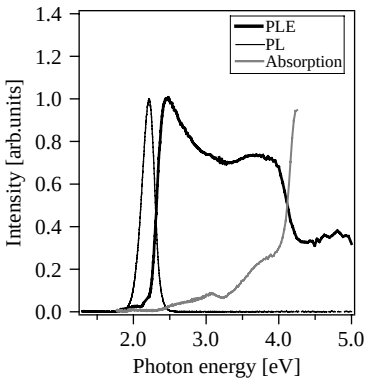

Fig. 4. Excitation and absorption spectra of $Ca_{0.99}Eu_{0.01}Ga_2S_4$ together with a photoluminescence spectrum.

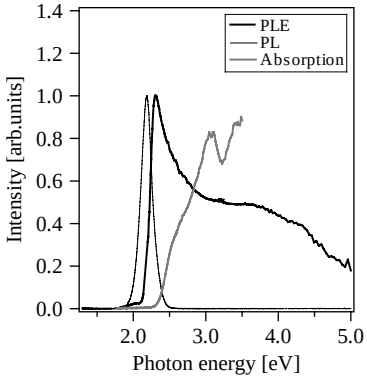

Fig. 5. Excitation and absorption spectra of $Ca_{0.90}Eu_{0.10}Ga_2S_4$ together with a photoluminescence spectrum.

between $x=0$ and 0.25, but shifted to the high energy side at the composition larger than $x=0.25$. The energy shift amounted to 50 meV at $x=1.0$ (see Fig. 2). The reduction of PL intensities at higher concentration above 25 mol% Eu may be due to the concentration quenching. When all Ca is substituted by Eu, the distance between Eu atoms is estimated as approximately 5 Å from the X-ray data. As the distance between Eu atoms at $x=0.25$ is estimated as 7 Å, assuming that the Eu atoms are homogeneously distributed, the interaction between the substituted Eu ions may take places at that concentration, resulting in the peak shift and concentration quenching as well.

Fig. 4 shows excitation and absorption spectra of $Ca_{0.99}Eu_{0.01}Ga_2S_4$ (1.0 Eu mol.%) together with photoluminescence (the peaks of PL and PLE are normalized to 1.0). The excitation spectrum has a maximum near the absorption edge at 2.5 eV and two peaks at 3.1 and 3.7 eV which correspond to those observed in the absorption spectrum, suggesting that the excited states consist of three levels being ascribed to the splitting of the 5d multiplets of a Eu ion. The PLE intensity decreases greatly above 4.0 eV, corresponding to the increase in the optical absorption. This is attributed to the strong light absorption just above the fundamental optical band edge of the host crystal.

Fig. 5 shows excitation and absorption spectra of $Ca_{0.90}Eu_{0.10}Ga_2S_4$ (10 Eu mol.%). The difference from that of the 1.0 Eu mol.% sample is that the steep decrease seen in the latter at 4.0 eV turned to a gradual one. As seen in Fig. 5, the optical absorption became stronger at the lower energy side, which was due to the absorption band around 2.5 eV presumably enhanced by the increase of the replaced Eu ions.

5. Conclusion

We have constructed the pseudo-binary phase diagram of the $CaGa_2S_4$–$EuGa_2S_4$ system by DTA and XRD analysis and shown that the system forms the complete solid solution, suggesting that the $Ca_{1-x}Eu_xGa_2S_4$ compounds can be grown at any value of x from 0 to 1. During the investigation above, more than 10 compounds with different values of x were synthesized in a same crystallographic phase. Using powders of these products, PL and PLE spectra were observed. And it was found that the most efficient compound for PL existed near $x=0.25$.

We have then grown $Ca_{1-x}Eu_xGa_2S_4$ single crystals at four x values ($x=0.01$, 0.02, 0.10 and 0.20), and their PL, PLE and optical absorption were observed. As x increased, a new absorption band appeared in the lower energy side below the intrinsic absorption edge. For small x values, the absorption is due to the deep band created by Eu doping. However, for larger value than $x=0.1$, it seems that a band-structure related absorption takes places, which should be confirmed by further experiments and/or by the theoretical band calculation [8]. PLE and absorption spectra have three peaks at the same energies of 2.5, 3.1 and 3.7 eV, suggesting that the excited states consist of three levels ascribed to the splitting of the 5d multiplets of Eu ions.

Acknowledgements

This work is partly supported by the grant for the high-technology research center project for private universities from ministry of education, sports, science, culture and technology, Japan.

References

[1] W.A. Barrow, R.C. Coovert, E. Dickey, C.N. King, C. Laakso, S.S. Sun, R.T. Tuenge, R. Wetross, J. Kane, SID Int. Symp. Dig. (1993).
[2] T.E. Pters, J.A. Baglio, J. Electrochem. Soc. 119 (1972) 230–236.
[3] P.C. Donohue, J.E. Hanlon, J. Electrochem. Soc. 121 (1974) 137–142.
[4] C. Hidaka, T. Takizawa, J. Cryst. Growth 237–239 (2002) 2009–2013.
[5] S. Iida, A. Kato, M. Tanaka, H. Najafov, H. Ikuno, Photoluminescence characterization of rare-earth stoichiometric compounds of $EuGa_2S_4$, J. Phys. Chem. Sol. 64 (2003) 1815–1819.
[6] Y.D. Jiang, G. Villalobos, J.C. Souriau, H. Paris, C.J. Summers, Z.L. Wang, Solid State Commun. 113 (2000) 475–478.
[7] S. Iida, T. Matsumoto, N.T. Mamedov, Y. Maruyama, A.I. Bairamov, B.G. Tagiev, O.B. Tagiev, R.B. Dzhabbarov, Jpn. J. Appl. Phys. 36 (1997) L857–L859.
[8] M. Ishikawa, T. Nakayama, Phys. Stat. Sol. (c) 1 (2004) 823.